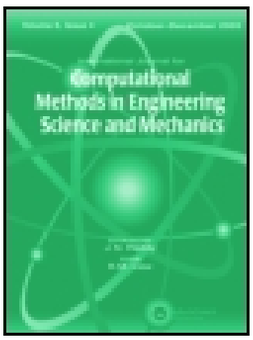

International Journal for Computational Methods in Engineering Science and Mechanics

ISSN: 1550-2287 (Print) 1550-2295 (Online) Journal homepage: http://www.tandfonline.com/loi/ucme20

Adaptive Isogeometric Analysis Based on a Combined r-h Strategy

Umesh Basappa, Amirtham Rajagopal & J. N. Reddy

To cite this article: Umesh Basappa, Amirtham Rajagopal & J. N. Reddy (2016): Adaptive Isogeometric Analysis Based on a Combined r-h Strategy, International Journal for Computational Methods in Engineering Science and Mechanics, DOI: 10.1080/15502287.2016.1153171

To link to this article: http://dx.doi.org/10.1080/15502287.2016.1153171

Accepted author version posted online: 23 Mar 2016.

Adaptive Isogeometric Analysis Based on a Combined *r*-*h* Strategy

Umesh Basappa[1], Amirtham Rajagopal*[1], and J. N. Reddy[2]

[1]Department of Civil Engineering, IIT Hyderabad, India
[2]Department of Mechanical Engineering , Texas A&M University, College Station, TX 77843-3123

Abstract

In the present work, an *r*-*h* adaptive isogeometric analysis is proposed for plane elasticity problems. For performing the *r*-adaption, the control net is considered to be a network of springs with the individual spring stiffness values being proportional to the error estimated at the control points. While preserving the boundary control points, relocation of only the interior control points is made by adopting a successive relaxation approach to achieve the equilibrium of spring system. To suit the non-interpolatory nature of the isogeometric approximation, a new point-wise error estimate for the *h*-refinement is proposed. To evaluate the point-wise error, hierarchical B-spline functions in Sobolev spaces are considered. The proposed adaptive *h*-refinement strategy is based on using De-Casteljau's algorithm for obtaining the new control points. The subsequent control meshes are thus obtained by using a recursive subdivision of reference control mesh. Such a strategy ensures that the control points lie in the physical domain in subsequent refinements, thus making the physical mesh to exactly interpolate the control mesh and thereby allowing the exact imposition of essential boundary conditions in the classical isogeometric analysis. The combined *r*-*h* adaptive refinement strategy results in better convergence characteristics with reduced errors than *r*- or *h*-refinement. Several numerical examples are presented to illustrate the efficiency of the proposed approach.

Keywords. Isogeometric analysis; hierarchical refinement; B-spline; *r*-*h* adaptive strategy

*Corresponding author email: rajagopal@iith.ac.in

1 Introduction

The concept of isogeometric analysis (IGA) advanced by Hughes et al. [1] is a novel tool for the analysis of partial differential equations. The primary objective is to map the physical domain exactly at coarse discretization and to simplify the refinement techniques by integration of Computer Aided Design (CAD) and Computer Aided Engineering (CAE). As a result, the method has received growing interest for many engineering problems [2, 3].

Mesh based methods (e.g., the traditional finite element method) are not desirable when applied to problems requiring remeshing and adaptive strategies. Finite element modelling of thin structures with large deformation, material discontinuities, and crack propagation requires remeshing to avoid highly distorted elements and to capture moving fronts. To overcome problems associated with the conventional FEM, various meshless techniques, for example, the smoothed particle hydrodynamics [4], the element-free Galerkin method (EFGM) [5, 6], the meshless Petrov Galerkin method (MLPG) [7], and the method of finite spheres [8] have been used. These methods have helped to achieve results which are devoid of mesh dependency. Although IGA is also a mesh based numerical method, unlike the C^0-continuous approximations (i.e., the Lagrange interpolation functions) used in FEM, splines used in IGA are smooth, piecewise polynomials with C^{p-1} continuity, where p is the order of the basis. These hierarchical basis functions help to perform mesh refinements to improve the solution in a seamless manner. Two main steps in an adaptive process include: (1) error estimation and (2) adaptive refinement based on the estimated error [9]. For the weak-form Galerkin finite element models, estimates of error can be obtained by recovery based methods, residual based methods, or goal-oriented methods. A more detailed review on these methods is presented by Ainsworth and Oden [10] and Babuska and Strouboulis [11]. The effectiveness of the adaptive refinement strategy relies on the accuracy of estimating the error in the numerical solution of the problem being solved.

Adaptive refinements in IGA have been studied by Hughes et al. [1]. In addition to the classical

h-refinement (knot insertion) and p-refinement (degree elevation), an efficient refinement technique called k-refinement (includes both knot insertion and degree elevation) has also been discussed by Hughes et al. [1]. The method involves an order elevation followed by the element discretization resulting in C^{p-1}-continuous function and is quite different from the C^0 functions introduced by classical p-refinement. The method was applied to elastic shell analysis and an improved convergence of solution was observed using the k-refinement (see [1]). Cottrell et al. [12] also studied the k-refinement to understand the smoothness of solution over classical C^0-continuous functions. The desirable properties of such adaptive IGA include convergence, regularity, compactness of support of basis functions and accurate representation of complex geometry on coarse grids. Refinement ($h \to 0$) implies convergence to the exact solution. While local refinement is preferred in practice, uniform refinement is the basis for standard convergence proofs. With regularity we aim at conforming methods with basis functions at least in $H^1(\Omega)$. In contrast to conventional FEM, additional global smoothness is regarded as beneficial.

The drawback of the tensor-product splines is that all refinements act globally. Any local refinement [13] requires a global refinement resulting in a number of control points associated with unwanted basis functions. For adaptive strategies hierarchical splines was presented by Forsey and Bartels [14]. Splines with varied knot line segments was presented in [15]. The research was later focused towards locally refinable tensor product splines [16]. T-splines (see [17, 18]) overcome such limitation by introducing locally refined T-junctions. T-splines are superior for making the transition from CAD to CAE seemingly more painless, but it also has superior properties from an exclusive design perspective or analysis perspective. It allows the designers to manipulate the complex models with far less control points than required by traditional non uniform rational B-splines (NURBS). Adaptive refinement studies using T-splines are made in [19]. The use of hierarchical splines for refinement is done in [20] and T-splines and LR B-splines[21] are used in some recent works ([22, 23, 24]). However, there is a need to overcome some limitations of the T-splines, in particular, with respect to the linear dependence of T-spline blending functions corresponding to

particular T-meshes [25]. The most recent development has been towards use of analysis suitable T-spline spaces [26] that are hierarchical in nature[27]. The hierarchical model allows complete local control of refinement by using a spline hierarchy whose levels identify subsequent levels of refinement for the underlying geometric representation. Recent studies have been towards estimating errors for very smooth functions. In this context, Cottrell et al. [28] have proposed an error estimation technique in a suitable Sobolev space. Xu et al. [29] have proposed a new error estimate based on a posteriori error estimation.

The essence of performing the *r*-refinement is to distribute the number of degrees of freedom in such a manner to obtain an optimal initial mesh so that accuracy of the solution obtained is the highest possible ([30], [31] and [32]). In the *r*-refinement for finite element method using hierarchical estimators the control point relocation procedure is based on the spring analogy approach (see [33] and [34]), where the stiffness of the spring is proportional to the error in solution. There have been several works on *r*-adaption based on material force method (see, for example, [35], [36], [37], [38], [39], [40], and [41]). There has been recent works on control point adjustment for B-spline curve approximation [42]. Various methods for parameterization of computational domain in isogeometric analysis in terms of control point locations has been studied and compared [43]. One of this includes *r*-adaption techniques based on residual error estimators together with a conjugate gradient algorithm for relocation of control points [43]. Two-dimensional domain decomposition based on skeleton computation for parameterization in isogeometric analysis has been made in [44]. The bounds on influence of domain parameterization and knot spacing on numerical stability in isogeometric analysis has been studied in [45].

There has been also hierarchical approaches to adaptive local refinement in isogeometric analysis [46]. Re-parameterization and shape optimization has recently been studied. Mapped B-spline basis functions are used for shape design and isogeometric analysis over an arbitrary parameterization [47]. A mesh regularization scheme to update internal control points for isogeometric shape design optimization has been proposed in [48]. High quality construction of analysis suit-

able trivariate NURBS solids by re-parameterization methods is made in [49]. Some fundamental aspects of shape optimization in the context of isogeometric analysis has been discussed in [50]. The physical mesh obtained in IGA by mapping of the parameter mesh is only end interpolatory to the control mesh. The reason is that the only end B-spline basis satisfies the Kronecker delta property for given open knot vector. In such cases we define control variables where degrees of freedom, boundary conditions, and geometry of physical domain are prescribed, unlike nodal variables in FEM. Such an description poses an issue in imposing Dirichlet (essential) boundary conditions exactly. Wang et al. [51] introduced a transformation method to relate both control and nodal variables to impose the essential boundary conditions. Bazilevs et al. [52] weakly enforced Dirichlet boundary conditions, which is shown to be effective. This issue is also observed in meshless methods, like moving least squares and reproducing kernel methods. Approaches like Lagrange multiplier [53], Transformation [54], and penalty [55] methods have also been used to impose essential boundary conditions.

In the present work, we propose a novel *r*-*h* adaptive isogeometric analysis for the numerical solution of plane elasticity problems. The *r*-adaptive strategy is based on relocation of the interior control point locations . The main aim of relocating the control points is to obtain an optimal control net. Such an optimal initial control net will ensure that the degrees of freedom defined at the control points are efficiently distributed, so that accuracy of the solution obtained is the highest possible, while preserving the exactness of the geometry. In this process only the interior control points are moved and the boundary control points are kept fixed. To this effect the control net is considered to be a network of springs with the spring stiffness being proportional to the error estimated by considering equilibrium at the global degrees of freedom defined at the control points. Equilibrium of spring system is achieved by considering a successive relaxation approach (see [34, 56, 57, 58]). The approach allows to relocate the control points towards the area of largest estimated error.

The *r*-adaption is followed by a *h*-refinement. A new error estimate for *h*-refinement is also

proposed in this work. Considering the non-interpolatory nature of the approximations in the isogeometric analysis, the classical approach to estimate the point-wise interpolation error in the Sobolev norm: $\boldsymbol{e} = \boldsymbol{u} - \boldsymbol{u}^h$ has been used with some modifications [59, 60]. To this effect, in the proposed method, hierarchical B-spline smooth functions in Sobolev space are considered to evaluate the error. The only requirement of Sobolev error estimation is the sufficient smoothness of function, u, to belong to an appropriate Sobolev space and is met by using hierarchical B-spline functions. The proposed estimator thus includes hierarchical B-spline functions as, $\tilde{u}$, together with $\tilde{u}^h$ as the solution to IGA.

An adaptive h-refinement strategy based on computed error is performed by using De-Casteljau's algorithm. Based on the proposed error estimator, the h-refinement is achieved through knot insertion in the parameter mesh. An updated control mesh is then obtained by using linear interpolation over the reference control mesh. The proposed method seeks for recursive subdivision algorithm to compute the new control points on the control mesh. The collection of such points is treated as subsequent control mesh which inherently includes the features of original geometry and hence, the physical mesh obtained through such a method preserves the original geometry. The algorithm allows finding points on the physical domain exactly. The physical mesh obtained from subsequent iterations interpolates the control mesh exactly through h-refinement, thereby avoids the use of additional procedures like Lagrange multipliers to impose essential boundary conditions. The combined r-h adaptive refinement strategy results in better convergence characteristics with reduced errors than r- or h-refinement alone. Numerical examples for the analysis of plane elasticity problems are considered for illustrating the use of the proposed method.

Following are the main contributions of the present work:

- A r-adaption procedure for IGA based on a spring analogy approach.
- An error estimate for h-refinement strategy in IGA. The displacement based error estimator is based on defining hierarchical B-spline smooth functions in Sobolev spaces.

- A novel refinement strategy based on De-Casteljau's algorithm for *h*-refinement. Such a procedure allows direct imposition of boundary conditions in the conventional IGA.

The paper is organized as follows. Section 2 is devoted to the univariate and multi-variate B-spline basis functions and nonuniform rational B-spline (NURBS). In Section 3 we define various Sobolev spaces and associated norms. Section 4 includes strong, weak, and matrix-vector form of the boundary value problem in the context of isogeometric analysis. The proposed method for error estimation in a Sobolev space are discussed in Section 5. Sections 5.1 and 6 deal with the *h*- and *r*-refinements. Numerical examples involving two-dimensional problems are presented in Section 7. Finally, in Section 8 we present a summary and discussion of the findings of the present study.

2 B-spline Basis functions and NURBS

Let K be a vector containing a non-descending sequence in parameter space, $K \in \mathbb{P}$, which is defined as

$$\begin{aligned} & K = \{\xi_1, \xi_2, ..., \xi_{n_k}\}, \quad \xi_i \in \mathbb{R} \\ \text{such that} \quad & \xi_i \geqslant \xi_{i-1} \qquad\qquad i = 2, 3, ..., n_k \end{aligned} \tag{1}$$

The vector K and scalar ξ_i are often termed as *knot vector* and *knots*, respectively, in computational geometry. Once we define the knot vector, the B-spline basis $N_i^p(\xi)$ of order $p > 0$ are computed

from constant basis using a recursive subdivision method.

$$\text{for } p = 0\,; \quad N_i^0(\xi) = \left\{ \begin{array}{ll} 1 & \text{if} \quad \xi \in [\xi_i, \xi_{i+1}) \\ 0 & \text{otherwise} \end{array} \right\}$$
$$\text{for } p > 0\,; \quad N_i^p(\xi) = \left\{ \begin{array}{ll} \frac{(\xi-\xi_i)}{(\xi_{i+p}-\xi_i)} N_i^{p-1}(\xi) + \frac{(\xi_{i+p+1}-\xi)}{(\xi_{i+p+1}-\xi_{i+1})} N_{i+1}^{p-1}(\xi) & \text{if} \quad \xi \in [\xi_i, \xi_{i+p+1}) \\ 0 & \text{otherwise} \end{array} \right\} \tag{2}$$

The B-spline basis for an arbitrary knot vector does not contain interpolation functions. In order to obtain interpolation functions, knots are required to be repeated, which is referred to as the knot multiplicity. In this regard, we introduce an open knot vector containing the end knot with knot multiplicity equal to $p + 1$. Further, B-spline basis includes other important properties such as:

- Partition of unity $\sum_{i=1}^{n_{cp}} N_i^p(\xi) = 1 \quad \forall \quad \xi \in [0, 1)$
- Non Negative $N_i^p(\xi) \geqslant 0 \quad \forall \quad \xi \in [0, 1)$
- Kronecker delta $N_i^p(\xi_j) = \delta_{ij} \quad \xi_j \in [\xi_i, \xi_{i+p+1})$

iff the knot multiplicity of ξ_j equal to order of curve

The standard geometries, such as a circle or ellipse, are best represented using rational functions. In this regard, we generalize the B-spline to rational polynomial referred as nonuniform rational B-splines (NURBS):

$$\mathrm{N}_i^p(\xi) = \frac{N_i^p(\xi) w_i}{\sum_{j=0}^{n_{cp}} N_j^p(\xi) w_j} \tag{3}$$

where w_i are the weights associated with the control points; we note that the number of weights and control points must match. We also note that the B-spline functions are recovered from NURBS by taking all weights equal to unity. A piecewise B-spline curve is constructed by taking a linear combination of the basis vectors $N_i^p(\xi)$ and the coefficients P_i, referred to as the control

points:

$$P(x) = \sum_{i=1}^{n_{cp}} N_i^p(\xi)\ P_i \tag{4}$$

The B-spline polynomials of order p have C^{p-1} continuous derivatives. If k represents knot multiplicity at knot ξ_i, then continuous derivative of polynomial gets reduced by C^{p-1-k} at that knot. Figure 1 shows the quadratic B-spline basis and polynomial curve for an assumed knot vector. The basis functions associated with control points P_1, P_4, and P_7 are interpolation functions as knots are repeated. It can also be seen in continuous derivative of B-spline polynomial. Polynomial have C^1-continuous derivative except at control points where knots are repeated making the continuity C^0, that is, at control point P_4.

A prior knowledge of univariate B-spline basis helps to define the basis in multi-dimension by making use of tensor product. Let d_p represent dimension of parametric space, $\mathbb{P}^{d_p}$. A knot vector defined in $\mathbb{P}^{d_p}$ is expressed as:

$$K_{\mathbf{i}} = \{\xi_1^\ell, \xi_2^\ell, ..., \xi_{n_k^\ell + p^\ell + 1}^\ell\} \quad \text{for} \quad \ell = 1, 2, ..., d_p \tag{5}$$

where n_k^ℓ and p^ℓ are the knot vector dimension and basis order in ℓ^{th} parametric direction. Let $N_i^{P^\ell}$, $i = 1, 2, ldots, n_{cp}^\ell$, be the univariate basis function defined in ℓ^{th} parametric direction. Multivariate basis function are then defined through tensor product and expressed as

$$B_{\mathbf{i}}^{\mathbf{P}}(\boldsymbol{\xi}) = \prod_{\ell=1}^{d_p} N_i^{p^\ell}(\xi^\ell) \tag{6}$$

where $\mathbf{i}$, $\boldsymbol{\xi}$ and $\mathbf{P}$ are the multi-index in parameter space. Finally, for a given control net $P_{\mathbf{i}} \in \mathbb{R}^d$, $P_{\mathbf{i}} = \{p_1^\ell, p_2^\ell, \ldots, p_{n_{cp}^\ell}^\ell\}$, the B-spline surface is defined as

$$P(\boldsymbol{x}) = \sum_{i=1}^{n_{cp}^\ell} B_{\mathbf{i}}^{\mathbf{P}}(\boldsymbol{\xi}) P_{\mathbf{i}} \tag{7}$$

3 Sobolev Spaces and Norms

Let Ω be an open bounded domain in $\mathbb{R}^d$ with a piecewise smooth boundary Γ. In order to study linear elliptic PDEs, we consider real-valued Sobolev spaces that are built on the function space $L^2(\Omega)$, where $L^2(\Omega)$ consists of functions that are square-integrable in the Lebesgue sense (see Reddy [61])

$$L^2(\Omega) = \{f : \int_\Omega f^2 d\Omega < +\infty\} \tag{8}$$

The space $L^2(\Omega)$ with the scalar product

$$(u, v)_{L^2(\Omega)} = \int_\Omega u\, v\, d\Omega,\ \ u,\ v \in L^2(\Omega) \tag{9}$$

and the associated norm $\| u \|_{L^2(\Omega)} = (u, u)^{1/2}_{L^2(\Omega)}$ becomes a Hilbert space. As an aid we first introduce concept of multi-index notation and the notion of a *weak derivative*.

Index notation

Let $\mathbb{Z}^n_+$ denote the set of all ordered n-tuples of non-negative integers : a member $\alpha \in \mathbb{Z}^n_+$ is denoted by $\alpha = (\alpha_1, \alpha_2, \ldots, \alpha_n)$, where each component α_i is a non-negative integer. The norm of α is given by$\| \alpha \| = \alpha_1 + \alpha_2 + \cdots + \alpha_n$ and the partial derivative $D^\alpha u$ is given by

$$D^\alpha u = \frac{\partial^{\|\alpha\|} u}{\partial x_1^{\alpha_1} \partial x_2^{\alpha_2} \ldots \partial x_n^{\alpha_n}} \tag{10}$$

Weak Derivative

We denote $C_0^\infty(\Omega)$ as the space of infinitely differentiable functions which are nonzero only on a compact subset of Ω. If $u \in L^2(\Omega)$ is a locally integrable function, we say that u possesses the (weak) derivative $v = D^\alpha u$ in $L^2(\Omega)$ provided that $v \in L^2(\Omega)$ and

$$\langle v, \phi \rangle = (-1)^{\|\alpha\|} \langle u, D^\alpha \phi \rangle\ \ , \forall \phi \in C_0^\infty(\Omega) \tag{11}$$

in the sense of distributions. The Sobolev space of order m, denoted by $\mathcal{H}^m(\Omega)$ is defined as the space consisting of those functions in $L^2(\Omega)$ that, together with all their weak partial derivatives up to order m, belong to $L^2(\Omega)$ (see Reddy [61])

$$\mathcal{H}^m(\Omega) = \left\{ u : D^\alpha u \in L^2(\Omega) \forall \parallel \alpha \parallel \leq m \right\} \tag{12}$$

The inner product $(.,.)^m_{\mathcal{H}}(\Omega)$ to make $\mathcal{H}^m(\Omega)$ an inner product space is defined by

$$(u, v)^m_{\mathcal{H}}(\Omega) = \sum_{\|\alpha\| \leq m} (D^\alpha u, D^\alpha v)_{L^2(\Omega)} \; for \; u, \; v \in \; \mathcal{H}^m(\Omega) \tag{13}$$

The inner product space induces the Sobolev norm $\| \cdot \|^m_{\mathcal{H}}(\Omega)$, which is defined as (see Reddy [61])

$$\| \; u \; \|^2_{\mathcal{H}^m(\Omega)} = (u, u)_{\mathcal{H}^m(\Omega)} = \sum_{\|\alpha\| \leq m} (D^\alpha u, D^\alpha u)_{L^2(\Omega)} \tag{14}$$

Let us consider a function $\boldsymbol{U}^h \in \mathfrak{S}^h = \{\boldsymbol{U}^h \in H^m(\Omega) \mid \boldsymbol{U}^h = \boldsymbol{u}_g \text{ in } \Gamma_u\}$ and $\boldsymbol{u}$ be a sufficiently smooth function $\boldsymbol{u} \in \mathfrak{S} = \{\boldsymbol{u} \in H^{>m}(\Omega) \mid \boldsymbol{u} = \boldsymbol{u}_g \text{ in } \Gamma_u\}$. The estimate on Sobolev error norm in general can be obtained using Eq. 14. The projection in Sobolev space in general is written as (see Reddy [61])

$$\|\boldsymbol{U}^h - \boldsymbol{u}\|_m = c_1 (h_e)^\alpha \; \|\boldsymbol{u}\|_r \tag{15}$$

where, $\alpha = \min(p + 1 - m, \; r - m)$

The above relation illustrates that the convergence rate is directly related to the order of polynomial basis, p, and element size, h_e. α, c_1, r and m are constants. The error in the in particular form for finite element method, solution can now be defined. Let $\boldsymbol{u}^h \in \mathfrak{S}^h = \{\boldsymbol{u}^h \in H^1(\Omega) \mid \boldsymbol{u}^h = \boldsymbol{u}_g \text{ in } \Gamma_u\}$ be the finite element solution function. We can then write

$$\|\boldsymbol{e}\|_m := \|\boldsymbol{u}^h - \boldsymbol{u}\|_m = c_2 (h_e)^\alpha \; \|\boldsymbol{u}\|_r \tag{16}$$

Unlike in finite element method, the NURBS functions used in IGA are not interpolatory in nature, but only interpolate at end control points. As a result, the analogy of Sobolev error estimates

used in interpolatory functions needs to be altered to get an estimate on error in IGA. This strong requirement in error estimation requires use of sufficiently smooth functions, $\boldsymbol{u}$, and meeting the continuity requirements as NURBS functions. One choice for such functions is by considering a hierarchical B-spline function, $\tilde{\boldsymbol{u}}$. Here in we mean that we use sufficiently smooth higher order B spline approximation functions that are recursively constructed from lower order B spline approximations as discussed in [14].

4 Boundary Value Problem

Consider a linear elastic material body occupying a geometric region Ω in real number space $\Omega \in \mathbb{R}^3$, as shown in Fig. 2. The boundary of the geometric region is denoted as Γ, such that $\Gamma = \Gamma_t \cup \Gamma_u$, where Γ_t denotes the part of the boundary where tractions $\mathbf{t}$ are prescribed and Γ_u is the portion of the boundary where displacements $\boldsymbol{u}_g$ are specified. The strong form of a boundary value problem considering Dirichlet (essential) and Neumann (natural) type boundary conditions can be stated as follows: find the displacement $\boldsymbol{u}(\boldsymbol{x})\Omega \mapsto \mathbb{R}^3$ such that the following equilibrium equation, Eq. (17), is satisfied:

$$\begin{aligned} & \boldsymbol{\nabla} \cdot \boldsymbol{\sigma} + \boldsymbol{f} = 0 \quad \text{in} \quad \Omega \\ \text{given} \quad & \boldsymbol{u} = \boldsymbol{u}_g \quad \text{on} \quad \Gamma_u \\ & \boldsymbol{\sigma n} = \boldsymbol{t} \quad \text{on} \quad \Gamma_t \end{aligned} \tag{17}$$

where $\boldsymbol{f}$ and $\boldsymbol{\sigma}$ denote the body force vector and stress tensor. For isotropic elastic material, the stress tensor is proportional to the gradient of the displacement via Hooke's law: $\boldsymbol{\sigma} = \boldsymbol{C} : \nabla \boldsymbol{u}$, where $\mathbf{C}$ the fourth-order linear elasticity tensor.

4.1 Galerkin Weak form

Consider a finite dimensional solution space $\mathfrak{S}^h$ and test space $\mathfrak{V}^h$ such that $\mathfrak{S}^h \subset \mathfrak{S}$ and $\mathfrak{V}^h \subset \mathfrak{V}$. Where $\mathfrak{S}$ and $\mathfrak{V}$ are the infinite dimension solution and test space. These finite dimensional space are defined as

$$\mathfrak{S}^h = \{\boldsymbol{u}^h \in H^p(\Omega) \mid \boldsymbol{u}^h = \boldsymbol{u}_g \text{ in } \Gamma_u\} \tag{18}$$

$$\mathfrak{V}^h = \{\boldsymbol{w}^h \in H^p(\Omega) \mid \boldsymbol{w}^h = 0 \text{ in } \Gamma_u\} \tag{19}$$

where $\mathcal{H}^p(\Omega)$ is a Hilbert space controlling regularity of the solution and the test fields. The interest is to find a finite dimensional solution field, $\boldsymbol{u}^h \in \mathfrak{S}^h$, such that it holds for all choices of finite dimensional test function, $\boldsymbol{w}^h \in \mathfrak{V}^h$, following the integral equation

$$\int_\Omega \boldsymbol{\nabla} \boldsymbol{w}^h : \boldsymbol{C} : \boldsymbol{\nabla} \boldsymbol{u}^h \, d\Omega = \int_\Omega \boldsymbol{w}^h \cdot \boldsymbol{f} \, d\Omega + \int_{\Gamma_t} \boldsymbol{w}^h \cdot \boldsymbol{t} \, d\Gamma \tag{20}$$

In an abstract manner we can write the Galerkin weak form as

$$a(\boldsymbol{w}^h, \boldsymbol{u}^h) = (\boldsymbol{w}^h, \boldsymbol{f}) + (\boldsymbol{w}^h, \boldsymbol{t})_\Gamma \tag{21}$$

Where, a$(\cdot, \cdot)$ represent a Bilinear form of trial and test function, $(\cdot, \cdot)$ is linear form of test function. Finite dimensional solution field and test function are approximated using B-spline basis as

$$\boldsymbol{u}^h = \sum_i B_i^P \boldsymbol{u}_i \qquad\qquad \boldsymbol{w}^h = \sum_j B_j^P \boldsymbol{w}_j \tag{22}$$

substituting Eq. 22 in Eq. 21 we get

$$\boldsymbol{w} a(\boldsymbol{B}^P, \boldsymbol{B}^P) \boldsymbol{u} = \boldsymbol{w} \, (\boldsymbol{B}^P, \boldsymbol{f}) + \boldsymbol{w} \, (\boldsymbol{B}^P, \boldsymbol{t})_\Gamma \tag{23}$$

$$\boldsymbol{w} \boldsymbol{K} \boldsymbol{u} = \boldsymbol{w}(\boldsymbol{f}_b + \boldsymbol{f}_t) \tag{24}$$

Where, $\boldsymbol{K} = a(\boldsymbol{B}^P, \boldsymbol{B}^P)$, $\boldsymbol{f}_b = (\boldsymbol{B}^P, \boldsymbol{f})$ and $\boldsymbol{f}_t = (\boldsymbol{B}^P, \boldsymbol{t})_\Gamma$ Eq. 24 is the matrix-vector form of the Galerkin weak form. The matrix-vector form has to hold for all possible choices of $\boldsymbol{w} \in \mathbb{R}^{n_e}$, which

results in force equilibrium equation as

$$\mathbf{KU} = \mathbf{F} \tag{25}$$

The solution to Eq. 25 will give the values of displacement vector **U**.

5 Error estimation in Isogeometric Analysis

5.1 *h*-refinement

Let $\tilde{\boldsymbol{u}}^h \in \mathfrak{S}^h = \{\tilde{\boldsymbol{u}}^h \in \mathcal{H}^p(\Omega) \mid \tilde{\boldsymbol{u}}^h = \boldsymbol{u}_g \text{ in } \Gamma_u\}$ and $\tilde{\boldsymbol{u}} \in \mathfrak{S}^h = \{\tilde{\boldsymbol{u}} \in H^{n>p}(\Omega) \mid \tilde{\boldsymbol{u}} = \boldsymbol{u}_g \text{ in } \Gamma_u\}$ be the hierarchical smooth B-spline function of higher order, recursively constructed from lower order basis functions. Following section refsec:3 we propose an estimate on error for Isogeometric analysis as

$$\|\boldsymbol{e}\|_m = \|\tilde{\boldsymbol{u}}^h - \tilde{\boldsymbol{u}}\|_m \tag{26}$$

We demonstrate in one dimension as to how the above estimate is acceptable. Fig. 3(a) illustrates the following terms: u_1 to u_5 are the nodally exact values , u is any very smooth function interpolating the nodally exact values. $\tilde{u}^h$ is the NURBS function obtained from nodally exact values as $\tilde{u}^h = N_i^p u_i$. $\tilde{u}$ is the hierarchical B-spline function obtained from same nodally exact values as $\tilde{u}^h = N_i^n u_i$. Now we increase the discretization. Figure 3(b) illustrates the same description for larger element discretization. It is observed that with increase in the discretization the hierarchical B-spline function matches the exact solution. These pictures clearly show that the solution converges as discretization of element increases (or element size decreases). Fig. 3(b) also clearly indicates that the error between NURBS and interpolatory function never approaches to zero value, even for a very larger element discretization. The reason for this is due to the non-interpolatory nature of NURBS function. But, it is observed that the error between NURBS and hierarchical B-spline function approaches to zero for larger element discretization, see Fig. 3(a) and (b). We

want to emphasize that we can get an estimate on error as the difference between NURBS function and hierarchical B spline functions as $\boldsymbol{e} = \tilde{\boldsymbol{u}}^h - \tilde{\boldsymbol{u}}$. The discretization of physical domain depends on the structure of knot vector, i.e. a non-zero knot span in parameter domain is mapped to an element in physical domain. Fig. 4 below illustrates the relation between them in one dimension. The knot vector considered for the example is $\{0, 0, 0, 1, 1, 1\}$. The non-zero knot span, i.e. $[\xi_3,\ \xi_4]$, correspond to one element discretization in physical domain. It is obvious that considering more number of non-zero knot span in parameter domain accounts for increase of element discretization in physical domain.

A non-zero knot span in a knot vector is obtained by process of independent knot insertion, i.e. not accounting for multiplicity of knot. The modified knot vector seeks for increased number of basis and control points. In the proposed method new control points are obtained by making use of linear interpolation over reference control points. This is given as

$$P_i^* = \frac{(\xi - \xi_i)}{(\xi_{i+1} - \xi_i)}\ P_i\ +\ \frac{(\xi_{i+2} - \xi)}{(\xi_{i+2} - \xi_{i+1})}\ P_{i-1} \quad \forall\ \xi \in [\xi_i,\ \xi_{i+2})$$

Figure 4(a) describes the B-spline curve interpolating only end control points as only the end basis satisfies the Kronecker delta property for open knot vector. The aforementioned method is adopted for *h*-refinement and is devoid of issues of relating the control variable to nodal variable. It has been reported that a direct imposition of displacement boundary condition to the control points results in significant error in the solution with deteriorated rates of convergence (see [51] and [52] for details). Similar situations are also seen in other mesh-less methods (see [62]). In the present work, the issue is best addressed by not considering any auxiliary methods to relate the control variables to the nodal variables in physical domain. In the proposed we can also extend the interpolation of reference control points, i.e. moving from linear interpolation to quadratic and so on. Figure 4(a)- (c) shows an example to describe the approach for *h*-refinement. It is seen from Fig. 4(c) that an introduction of a new non zero knot span results in an increase in the number of elements in the physical domain as seen in Fig. 4(a), together with a change in the basis as shown

in Fig. 4(b).

Figure 5(a) illustrates the one element discretization of physical domain. In the first step of *h*-refinement, the control points are not considered to be linear interpolation of reference control points. In the present method by using a recursive sub-division technique and using a elevation algorithm new control points which are on the physical domain are obtained from the reference control points. The new set of control points , P_i^*, obtained by making use of recursive sub-division algorithm over the reference control mesh is given by

$$P_i^* = \frac{(\xi - \xi_i)}{(\xi_{i+p} - \xi_i)} P_i + \frac{(\xi_{i+p+1} - \xi)}{(\xi_{i+p+1} - \xi_{i+1})} P_{i-1} \quad \forall\ \xi \in [\xi_i, \xi_{i+p+1})$$

Figure 5(b) and (c) are the five and ten element discretization of physical domain obtained by this procedure. It is clearly seen that the control points lie on the physical domain. Moreover, the geometry of the physical domain is also preserved.

To illustrate the proposed method of *h*-refinement a quarter segment of an annulus is considered (see Fig. 6(a)). A reference control net is considered to generate one element discretization of physical domain as shown in Fig 6(b). The physical domain interpolates only the end corner points. Using the proposed *h*-refinement makes the physical domain to exactly interpolate the control points at all locations, see Fig. 6(c) and (d). The geometry and continuity of the physical geometry is hence preserved and no other auxiliary methods are required for imposition of boundary conditions.

6 *r*-refinement

The proposed method is based on estimating the residual error. Following the defintion of error in equation26 and using the equations of equilibrium given in equation21 we obtain the equilibrium residual error. For any arbitrary approximation space $\mathcal{V} \in \mathcal{H}^{n>p}(\Omega)$ we have.

$$a(\boldsymbol{e}_m^h, \mathcal{V}) = (\tilde{\boldsymbol{u}}^h, \mathcal{V}) - (\tilde{\boldsymbol{u}}, \mathcal{V}) \tag{27}$$

$$= \sum_{N \in \Omega_{patch}} \int_N \boldsymbol{R}_N(\boldsymbol{x}) \mathcal{V}(\boldsymbol{x}) d\boldsymbol{x} \tag{28}$$

where N is the subpatch in the B-spline parametrization $\Omega_{patch}(\xi, \eta)$ of Ω. Using Cauchy-Schwartz inequality, together with following the propoerties of bilinear form $a(\cdot, \cdot)$ and using the approximation theory [10], we can obtain the residual based a-posterior error estimate in Isogeometric analysis as

$$\|\boldsymbol{e}_m^h\|^2 \leq C \sum_{N \in \Omega_{patch}} r_N^2 \|\boldsymbol{R}_N\|^2_{L^2(\Omega_{patch})} \tag{29}$$

where C is a constant and r_N is the diameter of the patch. The error function thus seeks for control point relocation (r-adaption) to the area of largest error quantity. A spring system is obtained by connecting a given set of control point to its neighboring control point through a pseudo spring whose stiffness is proportional to the computed error at that location. The compact support of basis functions at any control point, gives information about its neighboring control points. Let $e(\boldsymbol{x}_i)$ be a discrete value of error computed at global control point position, $\boldsymbol{x}_i$ for $i = 1, 2, ...n_{cp}$. The edge stiffness of spring, S_j for $j = 1, 2, ..., n_{spr}$, are defined as

$$K^j = \frac{e(\boldsymbol{x}_1^j) + e(\boldsymbol{x}_2^j)}{2} \tag{30}$$

where $\boldsymbol{x}_1^j$ and $\boldsymbol{x}_2^j$ are the local control point positions of spring, S_j. A linear system of equations can be arrived at each degree freedom of a control point as

$$\mathbf{K}^j \mathbf{x}^j = \mathbf{b}^j \Rightarrow \left\{ \begin{array}{l} K_{11}^j \boldsymbol{x}_1^j + K_{12}^j \boldsymbol{x}_2^j = \boldsymbol{b}_1^j \\ \\ K_{21}^j \boldsymbol{x}_1^j + K_{22}^j \boldsymbol{x}_2^j = \boldsymbol{b}_2^j \end{array} \right\} \tag{31}$$

Assembling the linear system of equation for each spring, S_j for $j = 1, 2, ..., n_{spr}$, results in global

equations expressed in abstract matrix-vector form as

$$\mathbf{KX} = \mathbf{B} \tag{32}$$

where $\mathbf{K}$ corresponds to global stiffness matrix of the spring system obtained by assembling the local stiffness matrices, $\mathbf{X}$ is unknown control point position vector required to be evaluated and $\mathbf{B}$ is global force vector which are nothing but discrete forces due to imbalance in equilibrium at each control point position. The new position of control points are computed by forcing the global force vector to zero, that is $\mathbf{B} = \mathbf{0}$, and solving for global control point position vector, $\mathbf{X}$.

$$\text{i.e.} \quad \mathbf{KX} = \mathbf{0} \tag{33}$$

In Fig. 7, consider Q and Q^* be the boundary points before and after deformation. The displacement vector, $\boldsymbol{u}$, gives the detail of displaced position of boundary points. Unit vector in normal and tangential direction to a surface boundary are denoted as, $\boldsymbol{n}_n$ and $\boldsymbol{n}_t$, such that $\boldsymbol{n}_n \cdot \boldsymbol{n}_t = 0$. Let $\mathbb{P}_n$ and $\mathbb{P}_t$ be the projection tensor which project vector along normal and tangential direction of surface boundary. The mathematical operation essential to convert singular algebraic equation, that is, Eq. (33), to non-singular algebraic equation is given as

$$\mathbb{P}_n \boldsymbol{u} = 0 \tag{34}$$

Equation (34) guarantees that the nodes located at corner retains its initial position and boundary nodes are allowed to displace only along surface boundary. The algebraic equation, Eq. (33), are solved using relaxation method, where the nodal points are updated iteratively as

$$\boldsymbol{x}^{new} = \boldsymbol{x}^{old} + \omega \, \frac{\sum_i (\boldsymbol{x}_i - \boldsymbol{x}^{old}) \, [\mathbf{K}_i(\boldsymbol{x}^{old}) - K_i(\boldsymbol{x}^{old})]}{\sum_i \mathbf{K}_i} \tag{35}$$

where, ω is a relaxation parameter arbitrarily chosen by trial and error procedure.

7 Numerical Examples

Numerical examples in two dimensional elasticity has been considered for demonstrating the proposed method. The numerical examples considered are: (a) Block under pressure (b) L- shape problem and (c) Infinite plate with a circular hole. The choice of control net made for each example is arbitrarily chosen so as to result in highest possible estimated error. The proposed method of error estimation and combined *r*-*h* refinement strategy has been implemented for all the examples. Firstly a relocation of control points is made based on spring analogy algorithm indicating a reduction in the solution error. This is then followed by $h-$ refinement. A comparison of convergence characteristics of of *h*- and *r*-*h* refinement has been done.

7.1 Block under pressure

Figure 8(a) illustrates the setup for block under pressure example. Where E is the young modulus and ν is poisson's ratio. The bottom edge of the block is restrained against both horizontal and vertical displacement and the top edge is subjected to uniform traction. The discretization of physical domain is illustrated in Fig. 8(d). Knot vector considered in both ξ and η direction are shown in Fig. 8(c), called as parameter mesh. The information of control points are shown in Fig. 8(b), called as control mesh. A non-zero knot span in parameter mesh and control point information in control mesh accounts for element discretization in physical domain. Fig. 8 illustrates the relation of control, parameter and physical mesh for element Ω_1.

An initial coarse physical mesh is considered for the *r*-refinement. Figure 9(a) shows the error plot measured as difference of IGA solution and hierarchical B-spline solution. A relocation of control points is made to understand the variation of error using spring analogy method. The method allows the control points to move towards the area of largest error. As a result, a reduction in L_2 error norm is observed [see Fig. 9(b)]. The error plot and physical mesh after *r*-refinement are shown in Figs. 10(a) and (b). These figures illustrate that in order to reduce the error in the

solution the geometry of physical mesh has to match with the gradient of the solution field.

Figures 11(a)–(e) are the physical meshes obtained after the *r*-refinement, termed as *r*-*h* refinement meshes. The same analogy is used to generate *r*-*h* meshes as in *h*-refinement operation, i.e. using recursive subdivision algorithm. The L_2 error norm plotted against degrees of freedom is shown in Fig 11(f). A comparison of *h*- and *r*-*h* are also shown. The convergence of solution for *r*-*h* are found better than the *h*-refinement. Figure 13 shows stress field plotted for block under pressure example after the $r-h$ refinement. This indicates that proposed strategy is best suited for obtaining flexible discretization.

7.2 Problem with L-Shaped Domain

An L-shaped domain of a specified geometry and subjected to a uniform pressure on two of its edges as shown in Fig. 14(a) is considered for the analysis. Figures 14(b) and (c) shows the control net and the parameter mesh in index shape. Here the control points at the re-entrant corner are repeated to achieve the L-shaped geometry. A typical element Ω_1 is marked on the physical mesh as shown in Fig. 14(d). An *r*-adaption procedure is performed on a initial coarse mesh. Figures 15(a) and (b) shows the physical mesh before and after *r*-adaption. There is a decrease in error norm with iterations and is shown in Figs. 15(c). The control point movement clearly indicates that the geometry of the physical mesh to matches the gradient of the solution field. The distribution of errors before and after relocation of the control points is shown in Fig. 16. A *r*-*h* adaption is performed on the relocated mesh and the meshes are shown in Fig. 17.

The final mesh obtained after combined *r*-*h* adaption cycles are shown in Fig. 18(a). A comparison of the percentages of the error norms for both *h*- and *r*-*h* refinements are shown in Fig. 18(b). The stress fields are shown in Fig. 19. These plots clearly indicate that there is a considerable decrease in the error when a combined refinement strategy is used.

7.3 Infinite plate with hole problem

A square plate with a circular hole, as shown in Fig. 20(a), is considered for the analysis (in this example a smooth geometry of the domain is considered for discretization). The control net, parameter mesh, and physical mesh are shown in Figs. 20(b)–(d).

The initial mesh considered is subjected to an *r*-adaption procedure based on the spring analogy. The resulting mesh is shown in Fig. 21(b). The error decreases with iteration as can be seen from Fig. 21(c). The distribution of errors before and after adaption is shown in Figs. 22(a)–(b). The *h*-adaptive meshes are shown in Fig. 23. The final mesh obtained after combined *r*-*h* adaption cycles are shown in Fig. 24. A comparison of the percentages of the error norm for both *h*- and *r*-*h* refinements is shown in Fig. 25(b). These plots clearly indicate that there is a considerable decrease in the error when a combined refinement strategy is used. The stress fields obtained from the combined $r - h$ strategy are shown in Fig. 26.

8 Conclusions

In the present work, an *r*-*h* adaptive isogeometric analysis is presented for the analysis of plane elasticity problems. The *r*-adaptive strategy is based on parameterization of arbitrarily chosen control point locations, that is, the control net is considered to be a network of springs. The spring stiffness is taken to be proportional to the discrete residual error estimated by considering equilibrium at the global degrees of freedom defined at the control points. Equilibrium of spring system is achieved by considering a successive relaxation approach. A new error estimate for the *h*-refinement has been derived. The classical approach to estimate the point-wise interpolation error, $\boldsymbol{e} = \boldsymbol{u} - \boldsymbol{u}^h$, in a Sobolev space cannot be directly applied to isogeometric analysis because the approximations are not interpolatory in nature. Therefore, in the proposed method hierarchical B-spline smooth functions are used to evaluate the interpolation error and there by the interpolation errors estimated are acceptable as the continuity properties are retained. An adaptive *h*-refinement

based on computed error is performed by using the De-Casteljau's algorithm for parameterization of the computational domain. The point-wise error estimation in Sobolev space as the difference of B-spline based solution and the hierarchical solution indicates the convergence of the solution with increase in the number of degrees of freedom. The method adopted for *h*-refinement which relates the control variable and nodal variable, illustrates that the rate of convergence is higher. The *r*-refinement based on the spring analogy illustrates that the geometry of control mesh is to follow the geometry of the solution field in order to reduce the error. The *h*-refinement followed by *r*-refinement shows better rate of convergence than only the *h*-refinement.

References

[1] T. J. R. Hughes, J. A. Cottrell, and Y. Bazilevs. Isogeometric analysis: CAD, finite elements, NURBS, exact geometry, and mesh refinement. *Computer Methods in Applied Mechanics and Engineering*, 194:4135–4195, 2005.

[2] Y. Bazilevs, V. M. Calo, T. J. R. Hughes, and Y. Zhang. Isogeometric fluid structure interaction: Theory, algorithms, and computations. *Computational Mechanics*, 43:3–37, 2008.

[3] H. Gomez, V.M. Calo, Y. Bazilevs, and T.J.R. Hughes. Isogeometric analysis of the Cahn-Hilliard phase-field model. *Computer Methods in Applied Mechanics and Engineering*, 197:4333–4352, 2008.

[4] J.J. Monaghan. Smoothed particle hydrodynamics : Theory and applications to non - spherical stars. *Monthly notices of the Royal Astronomical Society*, 181:375–389, 1977.

[5] W. K. Liu, S. Jun, and Y. F. Zhang. Reproducing kernel particle method. *International Journal for Numerical Methods in Fluids*, 20:1081–1106, 1995.

[6] T. Belytschko, Y. Y. Lu, and L. Gu. Element free Galerkin method. *International Journal for Numerical Methods in Engineering*, 37:229–256, 1994.

[7] S. N. Atluri and T. Zhu. A new meshless Petrov - Galerkin approach in computational mechanics. *Computational Mechanics*, 22(2):117 – 127, 1998.

[8] K.J. Bathe and S. De. Towards an efficient meshless computational technique: The method of finite spheres. *Engineering with Computers*, 18:170 – 192, 2001.

[9] J.N. Reddy. *An Introduction to finite element method*McGraw Hill, 3rd edition, Delhi, 2005.

[10] M. Ainsworth and J.T. Oden. *a-posteriori error estimation in FEM*. 2002.

[11] I. Babuska and T. Strouboulis. *The finite element method and its reliability, Numerical Mathematics and Scientific computation*. Clarendon Press, 2001.

[12] J. A. Cottrell, T. J. R. Hughes, and A. Reali. Studies of refinement and continuity in isogeometric structural analysis. *Computer Methods in Applied Mechanics and Engineering*, 196:4160–4183, 2007.

[13] S. Kleiss, B. Juttler, and W. Zulehner. Enhancing isogeometric analysis by a finite element based local refinement strategy. *Computer Methods in Applied Mechanics and Engineering*, 213- 216:168–182, 2012.

[14] D.R. Forsey and R. H. Bartels. Hierarchical B-spline refinement. *ACM Computer Graphics*, 22(4):205–212, 1988.

[15] F. Weller and H. Hagen. *Tensor product spline spaces with knot segments*. Vanderbilt University Press, Nashville, 1995.

[16] A. Bakenov. *T: Splines : Tensor product B- spline surfaces with T - Junctions*. Maters Thesis, Brigham Young University, 2001.

[17] T. W. Sederberg, J. Zheng, A. Bakenov, and A. Nasri. T-splines and T-NURCCS. *ACM Transactions on Graphics*, 22:477–484, 2003.

[18] T. Bazilevs, V. M. Calo, J. A. Cottrell, J. A. Evans, T. J. R. Hughes, S. Lipton, M. A. Scottand, and T. W. Sederberg. Isogeometric analysis using T-splines. *Computer Methods in Applied Mechanics and Engineering*, 199:229–263, 2010.

[19] M. A. Scott, X. Li, T. W. Sederberg, and T. J. R. Hughes. Local refinement of analysis-suitable T-splines. *Computer Methods in Applied Mechanics and Engineering*, 213-216:206–222, 2012.

[20] L.Tian, F. Chen, and Q. Du. Adaptive finite element methods for elliptic equations over hierarchical T- meshes. *Journal of Computational and Applied Mathematics*, 236:878–891, 2011.

[21] K.A. Johannessen, T. Kvamsdal, and T. Dokken. Isogeometric analysis using LR B- splines. *Computer Methods in Applied Mechanics and Engineering*, 269:471–514, 2014.

[22] M. R. Dorfel, B. Juttler, and B. Simeon. Adaptive isogeometric analysis by local h-refinement with T-splines. *Computer Methods in Applied Mechanics and Engineering*, 199:264–275, 2010.

[23] Z. J. Wu, Z. D. Huang, Q. H. Liu, and B. Q. Zuo. A local solution approach for adaptive hierarchical refinement in isogeometric analysis. *Computer Methods in Applied Mechanics and Engineering*, http://dx.doi.org/10.1016/j.cma.2014.10.026.

[24] Y. Bazilevs, L. Beirao da Veiga, J. A. Cottrell, T. J. R. Hughes, and G. Sangalli. Isogeometric analysis : Approximation, stability and error estimates for h- refinemed meshes. *Mathematical Models and Methods in Applied Sciences*, 6:90–1031, 2006.

[25] A. Buffa, D. Cho, and G. Sangalli. Linear independence of the T-spline blending functions associated with some particular t- meshes. *Computer Methods in Applied Mechanics and Engineering*, 199:1437–1445, 2010.

[26] J. Deng, F. Chen, X. Li, C. Hu, Z.Yang, and Y. Feng. Polynomial splines over hierarchical T-meshes. *Graphical Models*, 70:76–86, 2008.

[27] X. Li, J. Deng, and F. Chen. Polynomial splines overgeneral T - meshes. *Visual Computer*, 26:277–286, 2010.

[28] J. A. Cottrell, A. Reali, Y. Bazilevs, and T. J. R. Hughes. Isogeometric analysis of structural vibrations. *Computer Methods in Applied Mechanics and Engineering*, 195:5257–5296, 2006.

[29] G. Xu, B. Mourrain, R. Duvigneau, and A Galligo. A new error assessment method in isogeometric analysis of 2D heat conduction problems. *Advanced Science Letters*, 4:400–407, 2011.

[30] M.S. Shephard, M.A. Yerry, and P. Baehmann. Automatic mesh generation allowing for efficient a- priori and a- posteriori mesh refinement. *Computer Methods in Applied Mechanics and Engineering*, 55:161–180, 1986.

[31] M.S. Shephard. An algorithm for defining a single near optimum mesh for different load cases. *Computer Methods in Applied Mechanics and Engineering*, 15:617–625, 1980.

[32] N. Kikuchi. Adaptive grid design methods for finite element analysis. *Computer Methods in Applied Mechanics and Engineering*, 55:129–160, 1986.

[33] J. Peraire, J. Perio, and K. Morgan. Adaptive remeshing for three-dimensional compressible flow computation. *Journal of Computational Physics*, 103:269–285, 1992.

[34] Pierre Beal, J. Kokoand, and R. Touzani. Mesh r-adaption for unilateral contact problems. *International Journal of Applied Mathematics and Computer science*, 12:9–16, 2002.

[35] M.Braun. Configurational forces induced by finite element discretization. *Proc. Estonian Acad. Sci. Phys. Math*, 46(1/2):24–31, 1997.

[36] R.Muller, D. Gross, and G. A. Maugin. Use of material forces in adaptive finite element methods. *Computational Mechanics*, 33:421–434, 2004.

[37] G. A. Maugin. Material forces concepts and applications. *Applied Mechanics Review*, 48(5):213–245, 1995.

[38] H. Askes, E. Kuhl, and P. Steinmann. An ALE formulation based on spatial and material settings of continuum mechanics. part 2: classification and applications. *Computer Methods in Applied Mechanics and Engineering*, 193:4223–4245, 2004.

[39] H. Askes, S.Bargmann, E. Kuhl, and P. Steinmann. Structural optimization by simultaneous equilibration of spatial and material forces. *Communications to Numerical Methods in Engineering*, 21:433–442, 2005.

[40] S. Riehl and P. Steinmannn. An integrated approach to shape optimization and mesh adaptivity based on material residual forces. *Computer Methods in Applied Mechanics and Engineering*, 278:640–663, 2014.

[41] J. Friederich, G. Leugering, and P. Steinmannn. Sensitivities for topological graph changes in finite element meshes and application to adaptive refinement. *Proc. Appl. Math. Mech*, 14:873–874, 2014.

[42] H. Yang, W. Wang, and J. Sun. Control point adjustment for B-spline curve approximation. *Computer aided design*, 36:639–652, 2004.

[43] G. Xu, B. Mourrain, R. Duvigneau, and A.Galligo. Parametrization of computational domain in Isogeometric analysis : methods and comparison. *Computer Methods in Applied Mechanics and Engineering*, 200(23-24):2021– 2031, 2011.

[44] J. Xu, F. Chen, and J. Deng. Two dimensional domain decomposition based on skeleton computation for parametrization and isogeometric analysis. *Computer Methods in Applied Mechanics and Engineering*, 284:541–555, 2015.

[45] E. Pilgerstorfer and B. Juttler. Bounding the influence of domain parametrization and knot spacing on numerical stability in Isogeometric analysis. *Computer Methods in Applied Mechanics and Engineering*, 268:589–613, 2014.

[46] A.V. Vuong, C. Giannelli, B. Juttei, and B. Simeon. A hierarchical approach to adaptive local refinement in Isogeometric analysis. *Computer Methods in Applied Mechanics and Engineering*, 200:3554–3567, 2011.

[47] X. Yuan and W. Ma. Mapped B- spline basis functions for shape design and isogeometric analysis over an arbitrary parametrization. *Computer Methods in Applied Mechanics and Engineering*, 269:87–107, 2014.

[48] M.J. Choi and S. Cho. A mesh regularization scheme to update internal control points for isogeometric shape design optimization. *Computer Methods in Applied Mechanics and Engineering*, 285:694–713, 2015.

[49] G. Xu, B. Mourrain, A. Galligo, and T. Rabczuk. High quality construction of analysis suitable trivariate NURBS solids by reparametrization methods. *Computational Mechanics*, 54(5):1303– 1313, 2014.

[50] D.Fuseder, B. Simeon, and A.V. Vuong. Fundamental aspects of shape optimization in the context of Isogeometric analysis. *Computer Methods in Applied Mechanics and Engineering*, 286:313–331, 2015.

[51] D. Wang and J. Xuan. An improved NURBS-based isogeometric analysis with enhanced treatment of essential boundary conditions. *Computer Methods in Applied Mechanics and Engineering*, 199:2425–2436, 2010.

[52] Y. Bazilevs and T. J. R. Hughes. Weak imposition of Dirichlet boundary conditions in fluid mechanics. *Computers and Fluids*, 36:12–26, 2010.

[53] I. Kaljevic and S. Saigal. An improved element free Galerkin formulation. *International Journal for Numerical Methods in Engineering*, 40:2953–2974, 1997.

[54] J. S. Chen, C. T. Wu, and C. Pan. Application of reproducing kernel particle method to large deformation and contact analysis of elastomers. *Rubber Chemistry and Technology*, 71:191–213, 1998.

[55] T. Zhu and S. N. Atluri. A modified collocation method and a penalty formulation for enforcing the essential boundary conditions in the element free Galerkin method. *Computational Mechanics*, 21:211–222, 1998.

[56] A. Rajagopal, R. Gangadharan, and S. M. Sivakumar. A performance study on configurational force and spring-analogy based mesh optimization schemes. *International Journal for Computational Methods in Engineering Science and Mechanics*, 7(4):241–262, 2006.

[57] M. H. Afshar, M. Naisipour, and J. Amani. Node moving adaptive refinement strategy for planar elasticity problems using discrete least square meshless method. *Finite Elements in Analysis and Design*, 47:1315–1325, 2011.

[58] A. Rajagopal. *Mesh adaption for plane and plate bending problems*. Indian Institute of Technology Madras, India, 2006.

[59] S. C. Brenner and L. R. Scott. *The Mathematical Theory of Finite Element Methods*. Springer-Verlag, New York, 2008.

[60] G. Strang and G. J. Fix. *An Analysis of the Finite Element Method*. Prentice-Hall, Englewood Cliffs, N.J, 1973.

[61] J. N. Reddy. *Applied Functional Analysis and Variational Methods in Engineering*. McGraw-Hill, NY, 1986; reprinted by Krieger, Melbourne, FL, 1991.

[62] J. S. Chen and H. P. Wang. New boundary condition treatments in meshfree computation of contact problems. *Computer Methods in Applied Mechanics and Engineering*, 187:441–468, 2000.

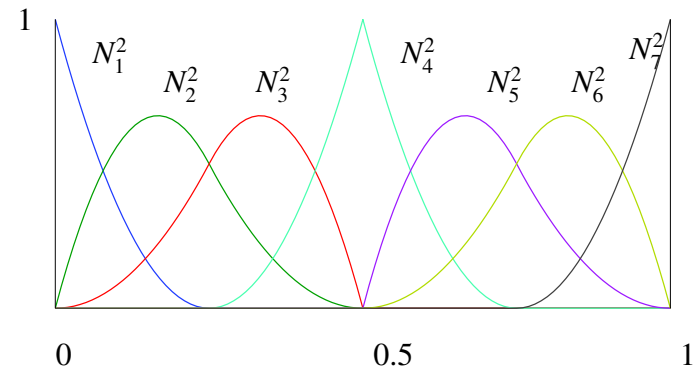

(a)

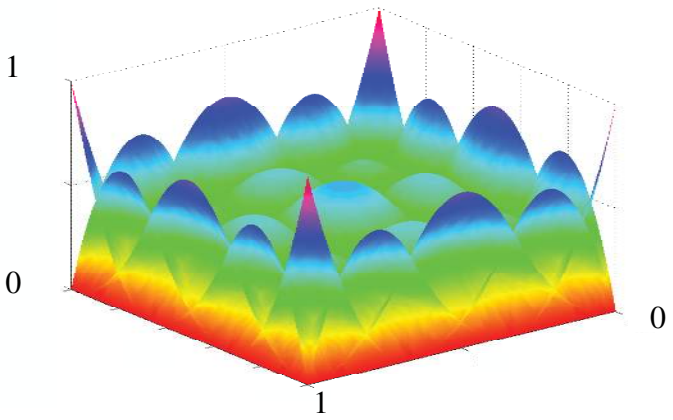

(b)

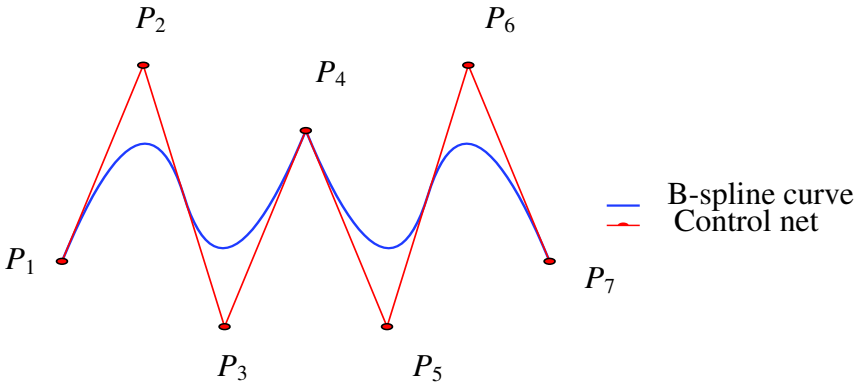

(c)

Figure 1: (a) B-spline basis functions of order 2 (b) B-spline basis functions of order 2 in two dimensions for a knot vector $K = \{0, 0, 0, 1/4, 2/4, 2/4, 3/4, 1, 1, 1\}$ (c) Control net and B-spline curve

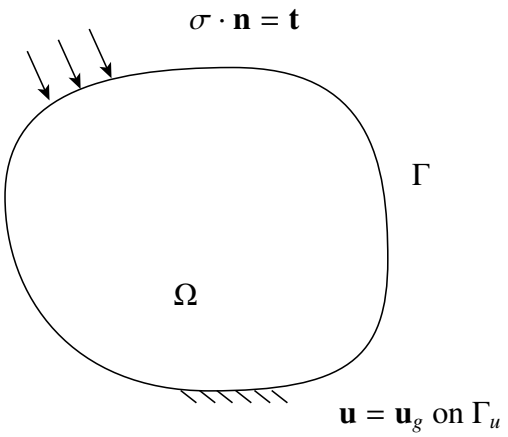

Figure 2: Two dimensional elastic body under consideration

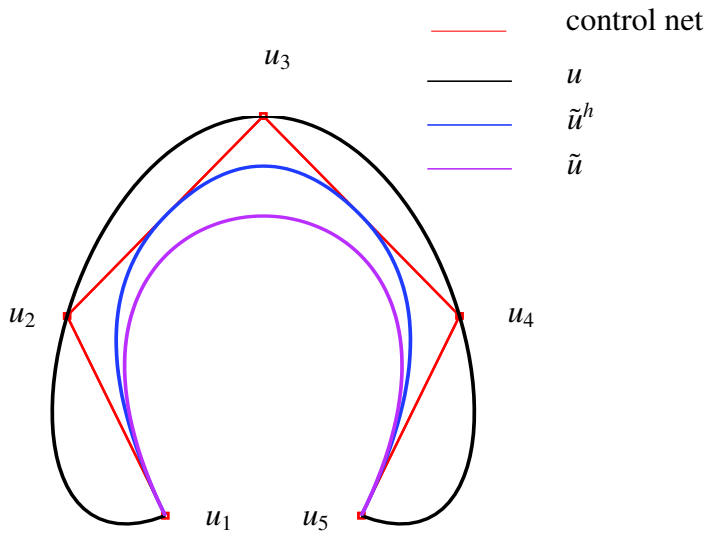

(a)

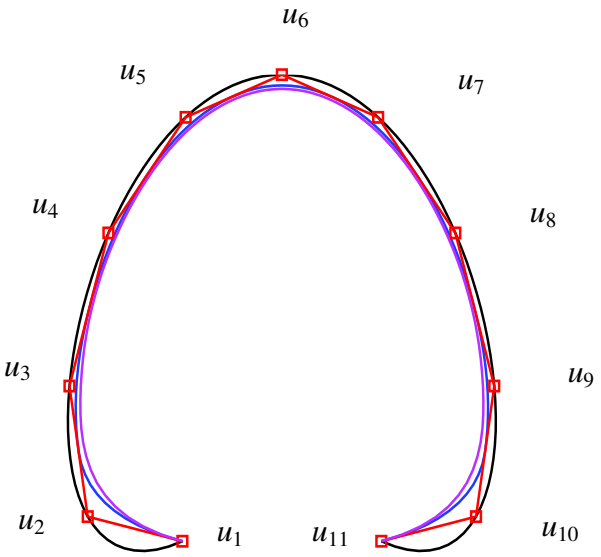

(b)

Figure 3: Description of progressive hierarchical B - spline for error estimation in IGA

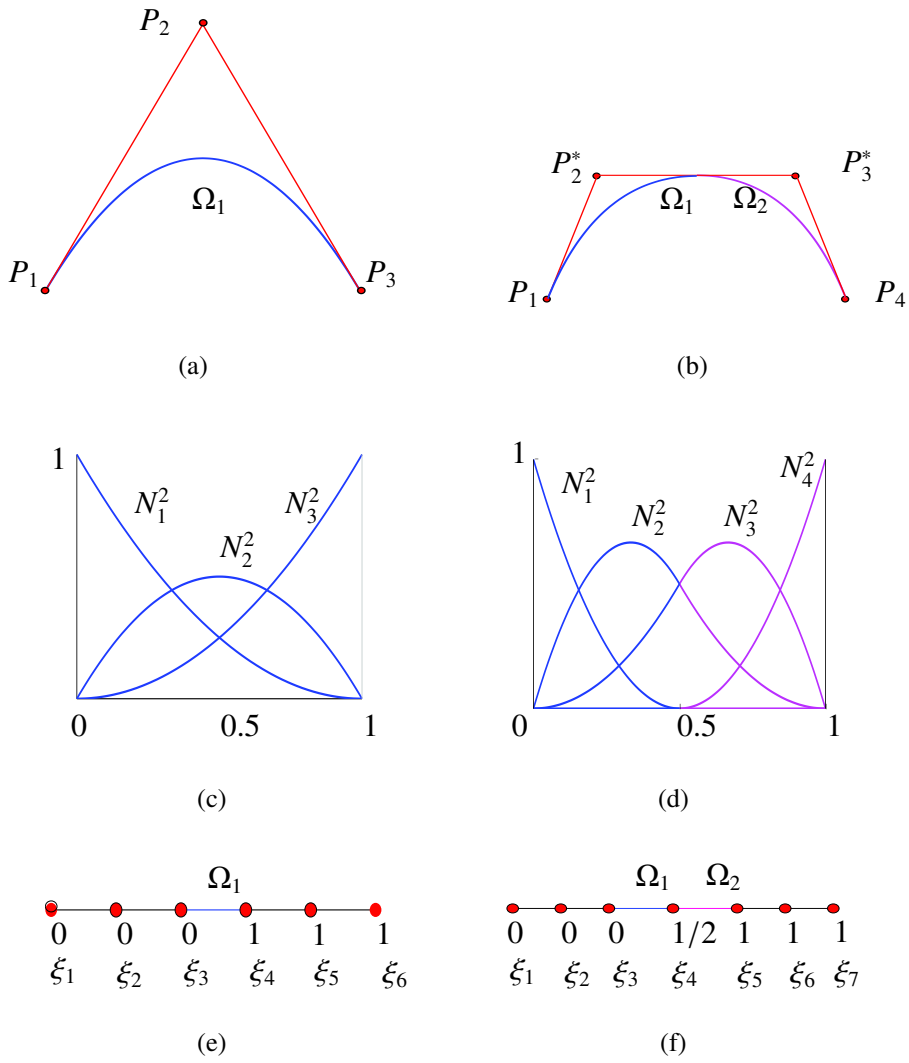

Figure 4: Approach for *h*-refinement in IGA (a) One element discretization (b) Two element discretization (c) Quadratic B- spline basis for one element discretization (d) Quadratic B- spline basis for two element discretization (e) Parametric domain for one element (f) Parametric domain for two elements

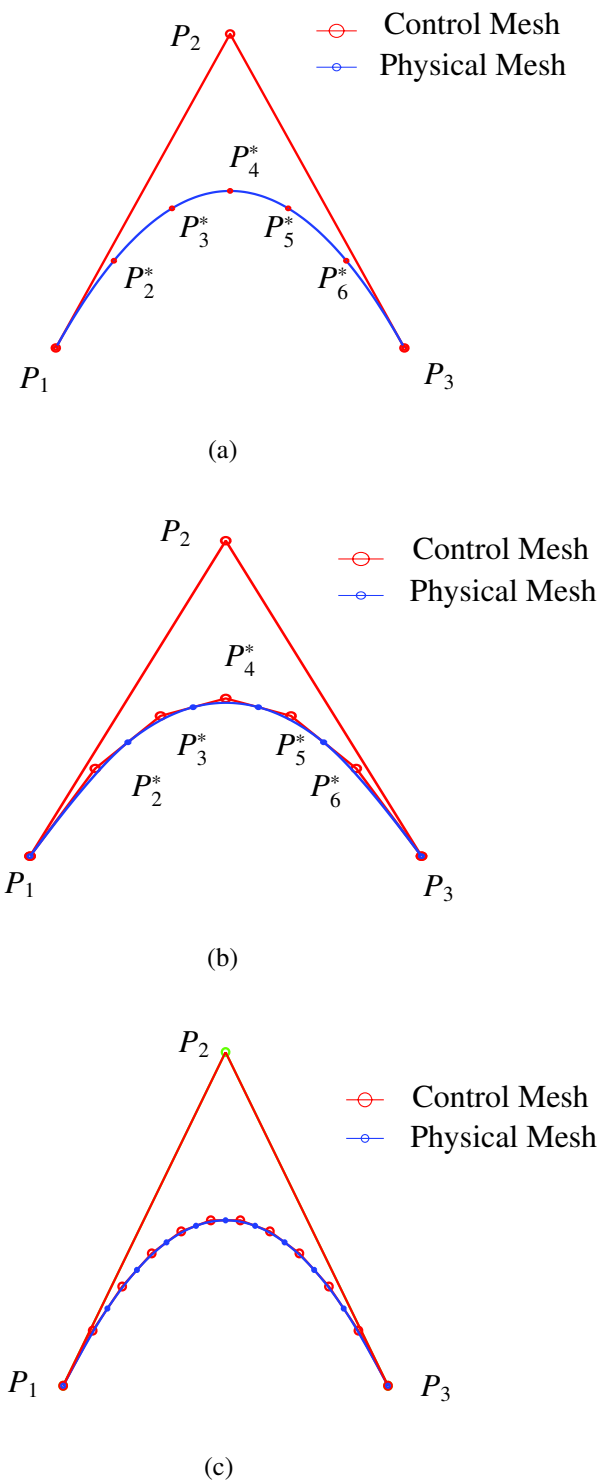

Figure 5: Adaptive *h*-refinement in IGA. (a) One element discretization. (b) Five element discretization. (c) Ten element discretization.

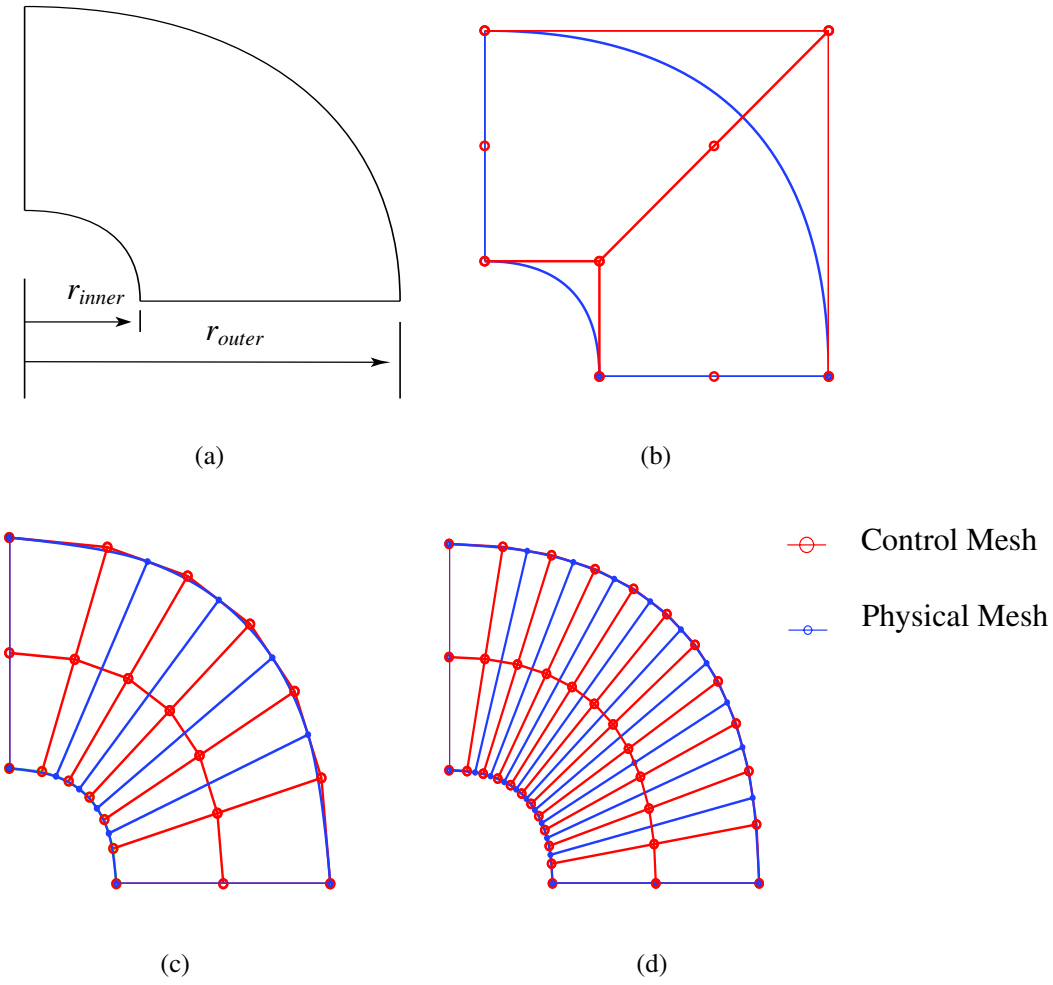

Figure 6: Adaptive *h*-refinement in IGA (a) Annulus Example (b) One element discretization (c) Five element discretization (d) Ten element discretization

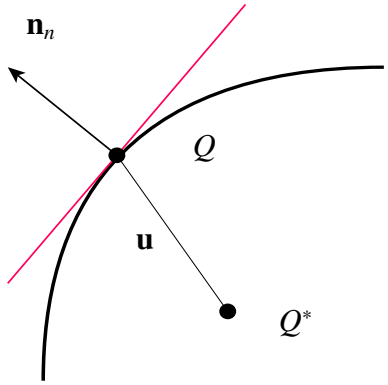

(a)

Figure 7: Boundary condition in $r-$ adaption

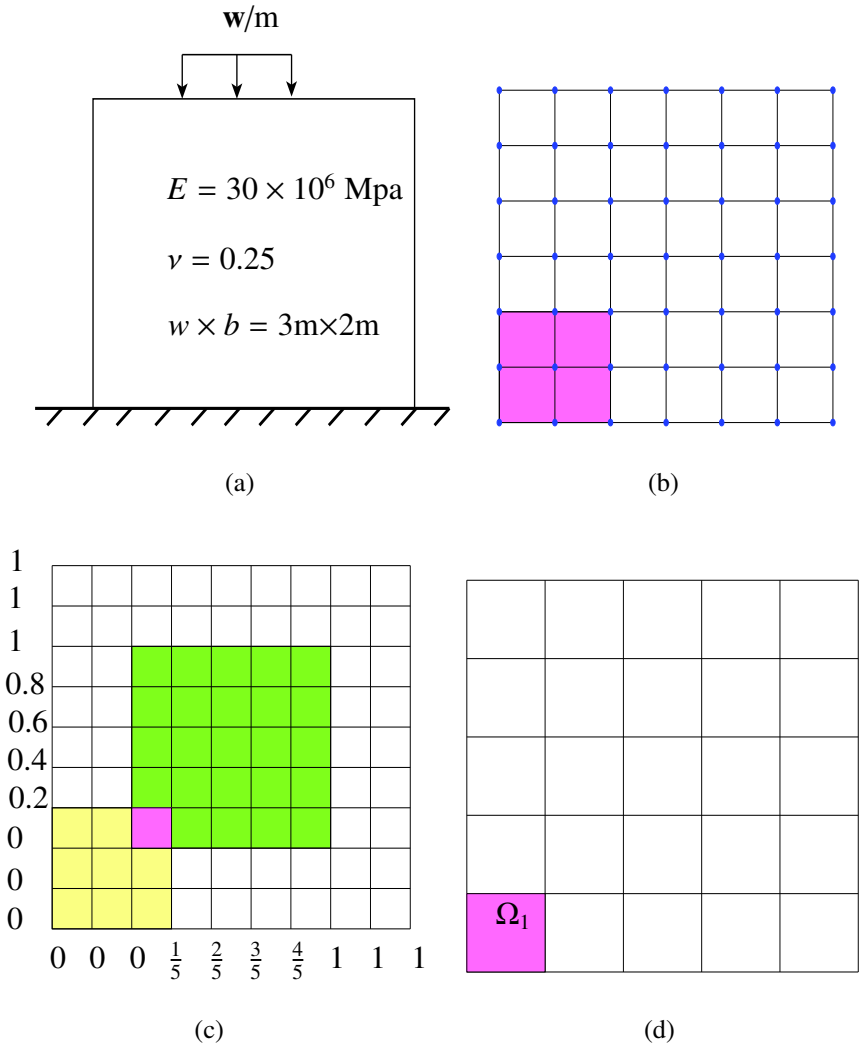

Figure 8: Block under pressure example (a) Physical domain (b) Control net or mesh (c) Parameter mesh in Index space (d) Physical mesh over the physical domain

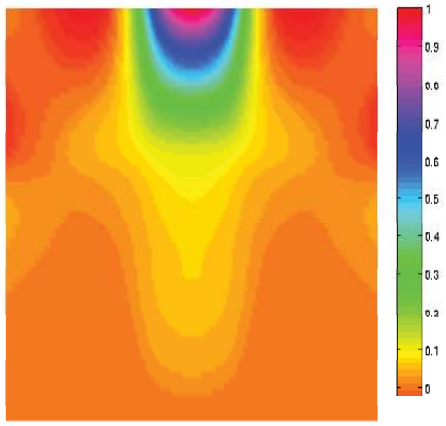

(a)

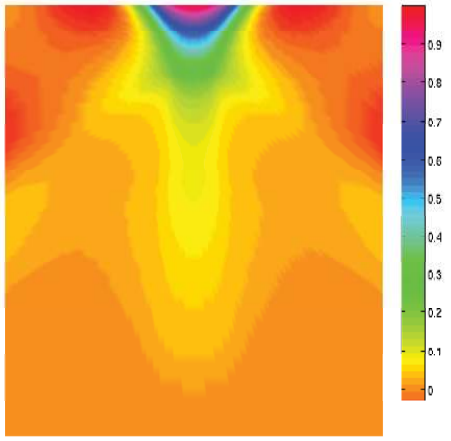

(b)

Figure 9: *r*-refinement for block under pressure example (a) Error plot before *r*-adaption (b) Error norm in *r*-adaption

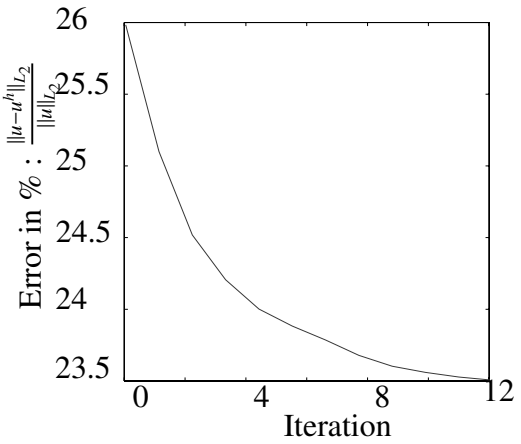

(a)

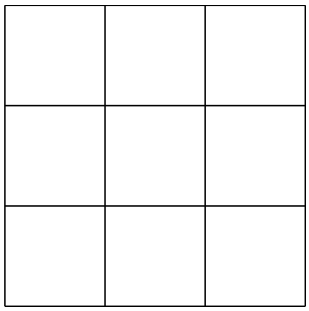

(b)

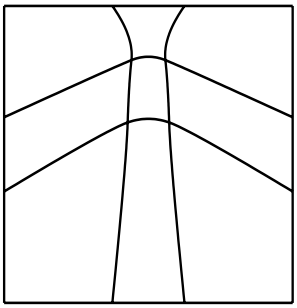

(c)

Figure 10: (a) Error plot after *r*-adaption (b) Physical mesh before *r*-adaption (c) Physical mesh after *r*-adaption

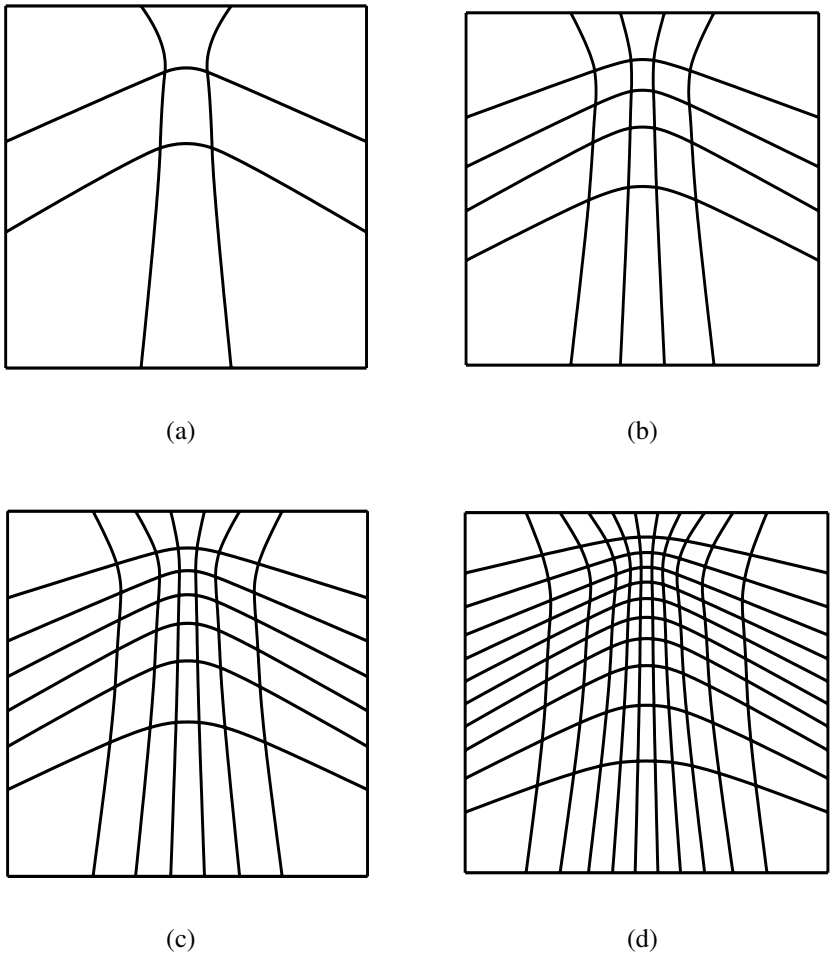

Figure 11: *r-h* refinement meshes for block under pressure example

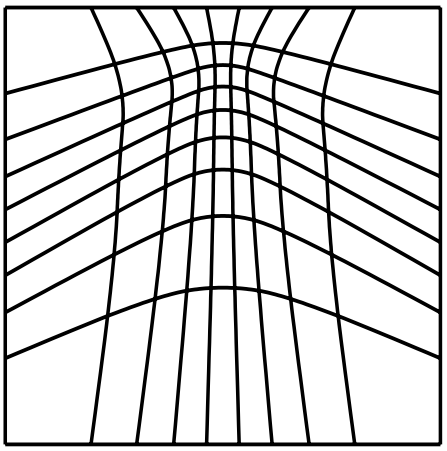

(a)

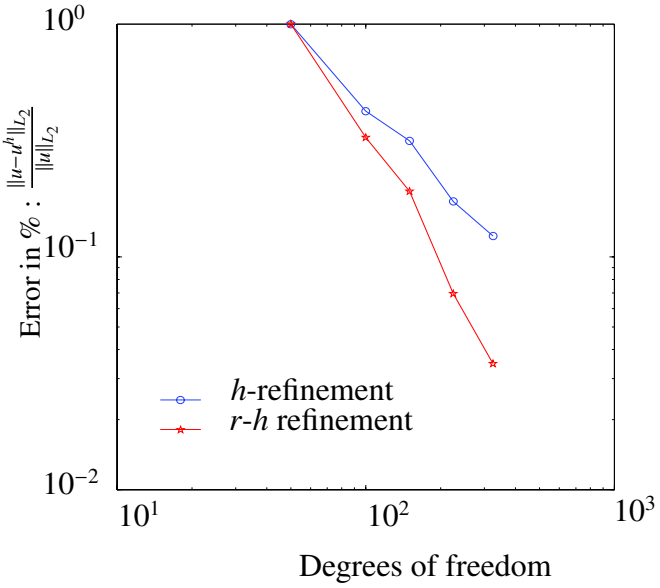

(b)

Figure 12: (a) Final *r*-*h* refinement mesh and (b) Comparison of error norm for *h*- and *r*-*h* refinement

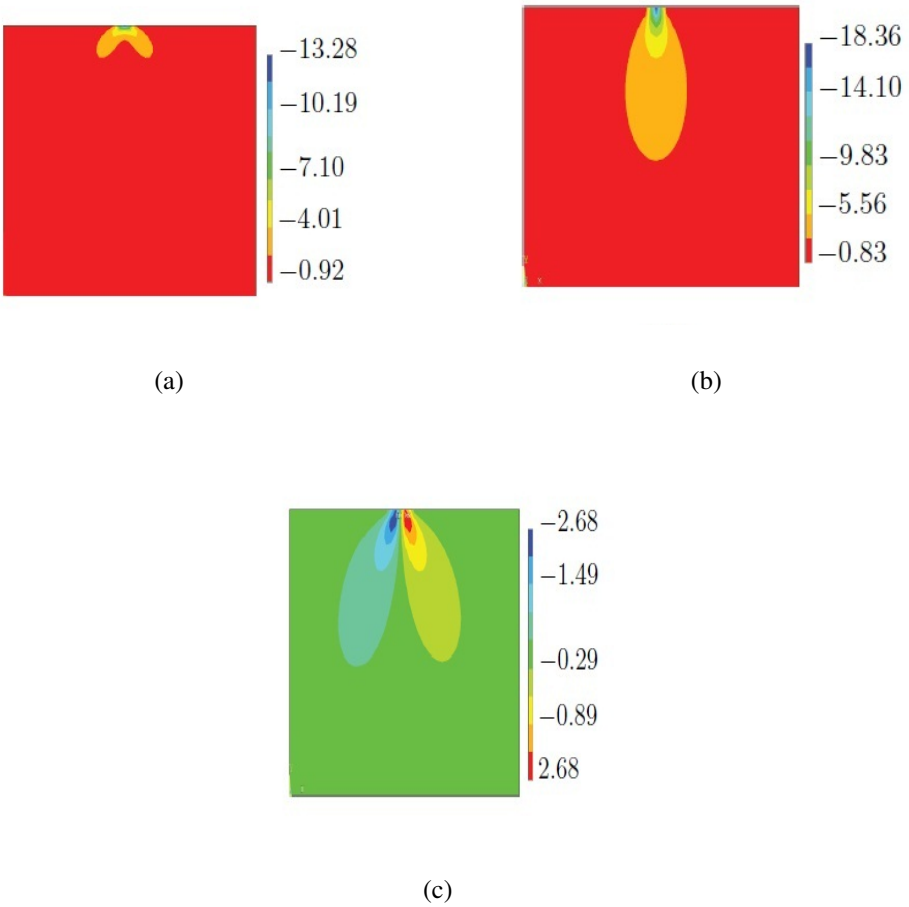

(a) (b)

(c)

Figure 13: Block under pressure example (a) Distribution of stress $\sigma_x x$ (b) Distribution of stress σ_{yy} (c) Distribution of stress σ_{xy} obtained from the final adapted mesh

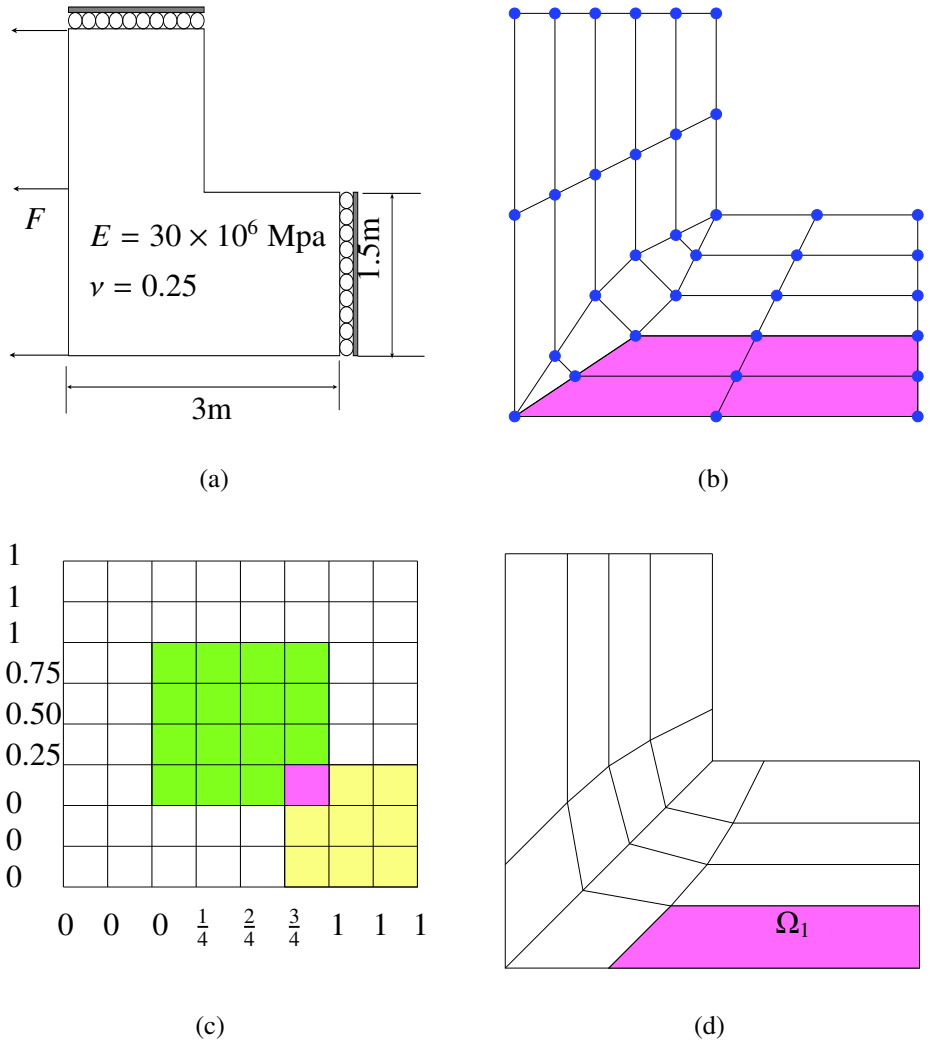

Figure 14: L Shaped domain (a) Physical domain (b) Control net or mesh (c) Parameter mesh in Index space (d) Physical mesh over the physical domain

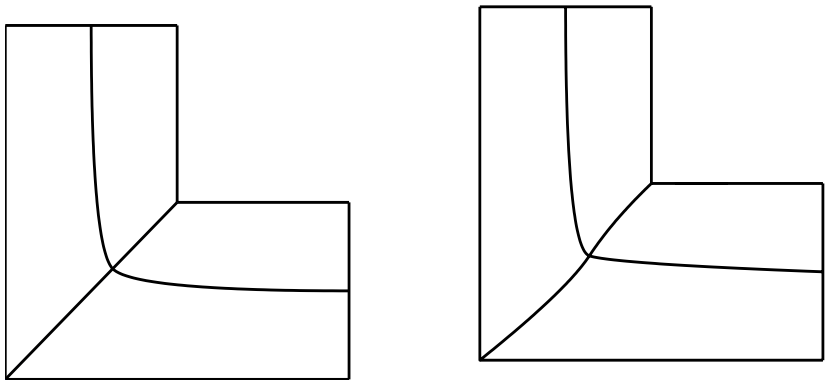

(a) (b)

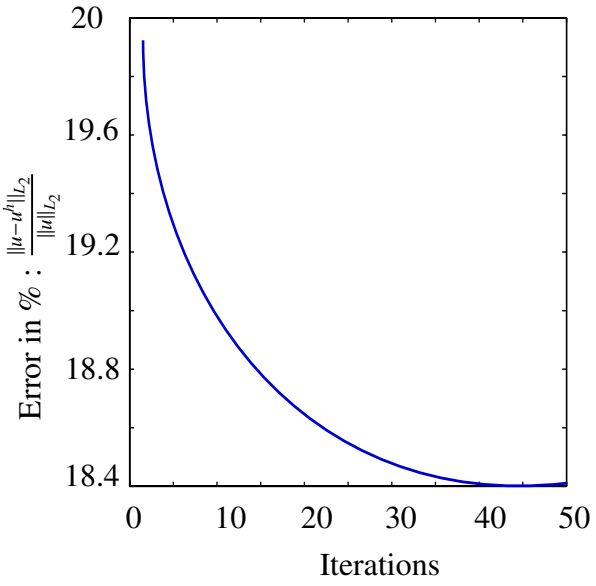

(c)

Figure 15: *r*-refinement for L-shaped domain (a) Physical mesh before *r*-adaption (b) Physical mesh after *r*-adaption (c) Error norm percentage with iterations.

(a)

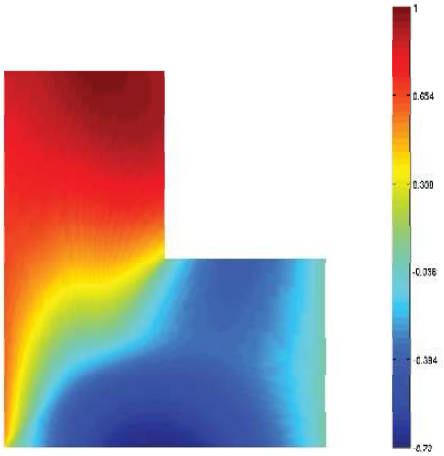

(b)

Figure 16: *r*-refinement for L-shaped domain (a) Error plot before *r*-adaption (b) Error norm plot after *r*-adaption

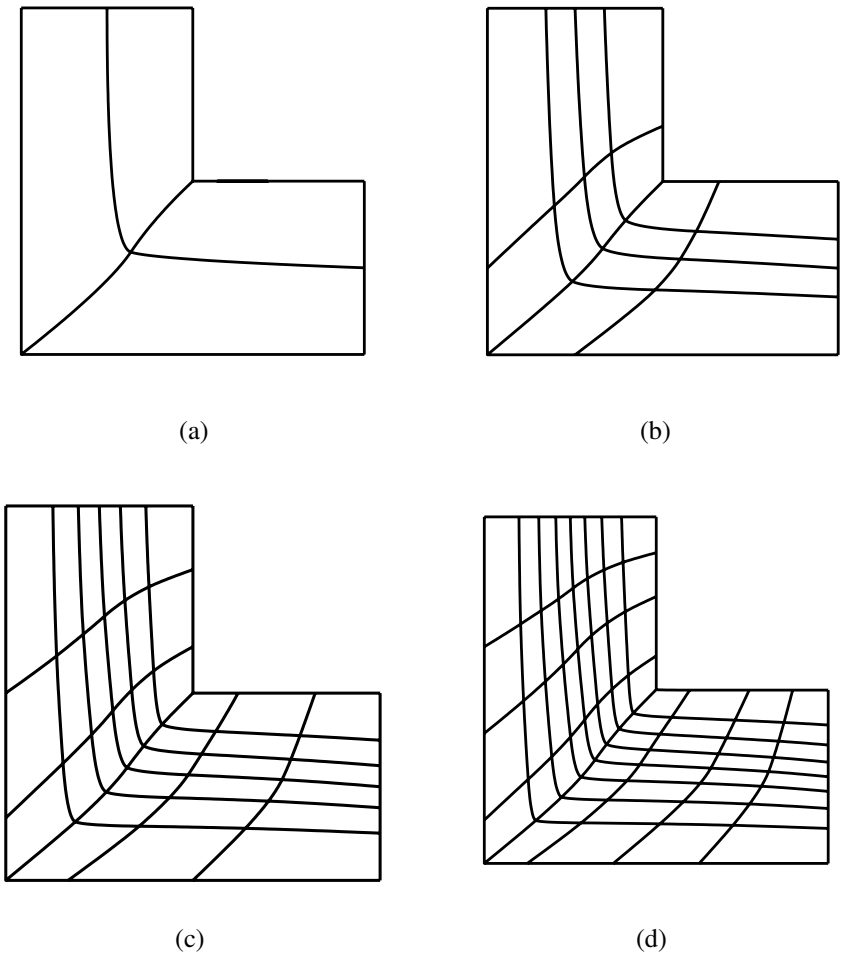

Figure 17: *r-h* refinements for L-shaped domain.

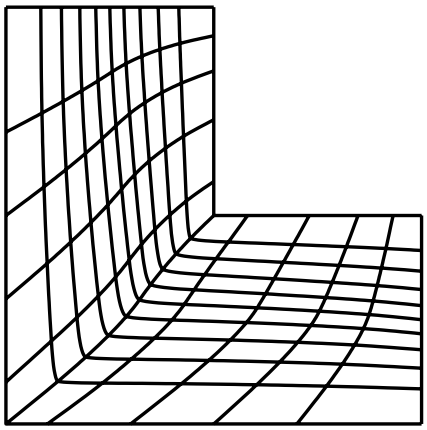

(a)

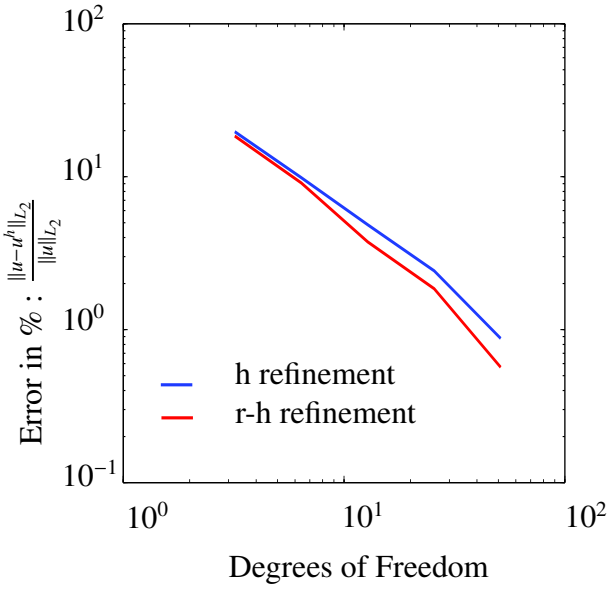

(b)

Figure 18: (a) Final *r*-*h* refinement mesh for L-shaped domain (b) Comparison of error norm for *h*- and *r*-*h* refinement

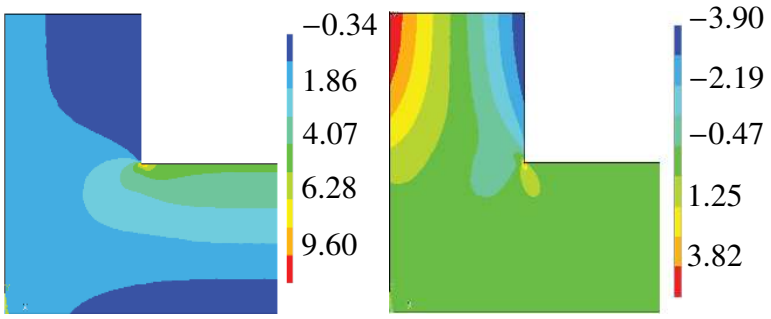

(a) (b)

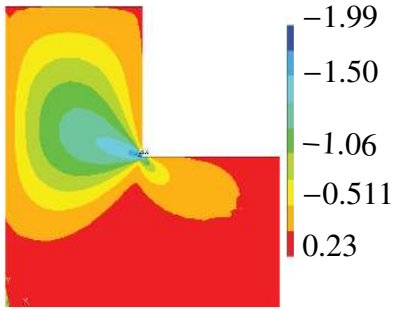

(c)

Figure 19: L shaped example (a) Distribution of stress $\sigma_x x$ (b) Distribution of stress σ_{yy} (c) Distribution of stress σ_{xy} ontained from the final adapted mesh

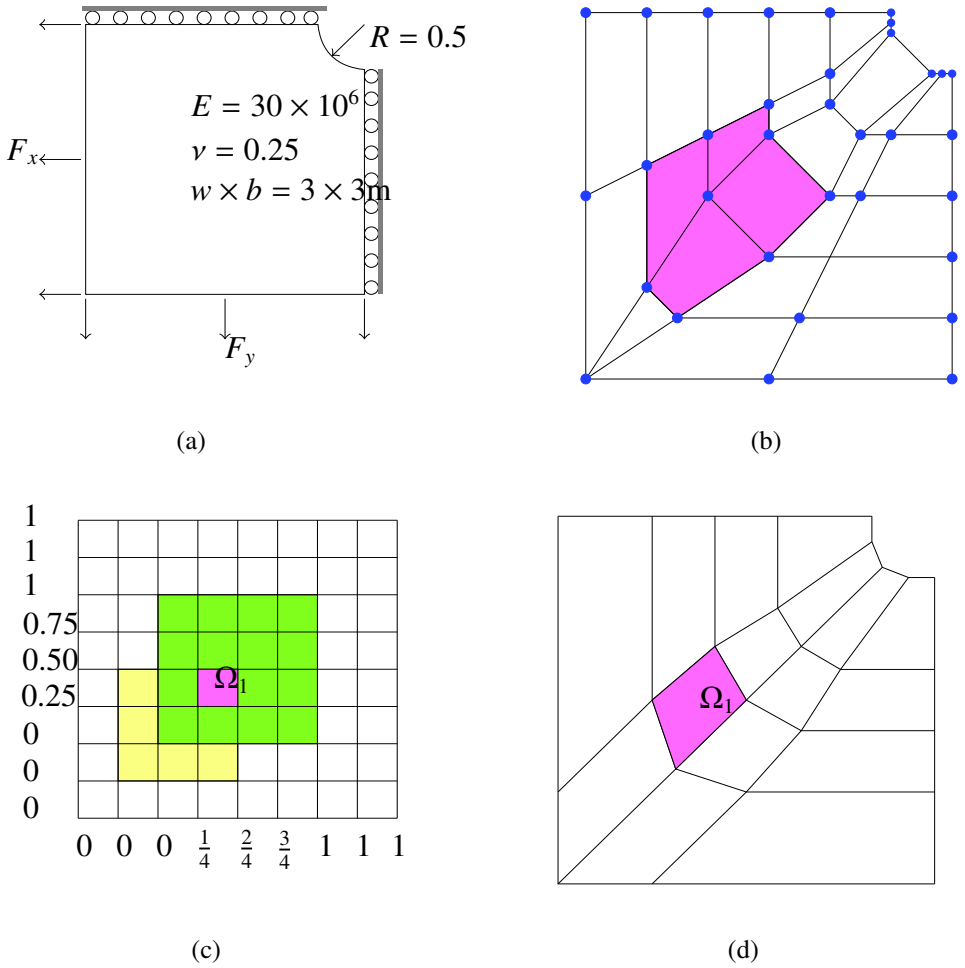

Figure 20: Plate with a circular hole example (a) Physical domain (b) Control net (c) Parameter mesh (d) Physical mesh

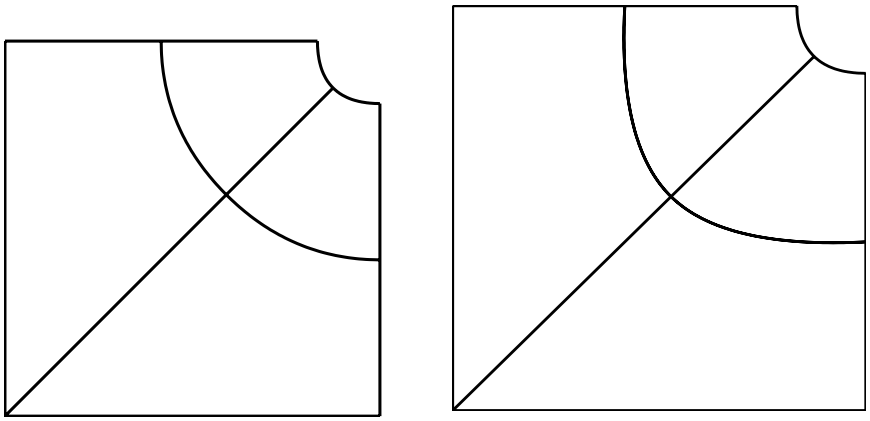

(a) (b)

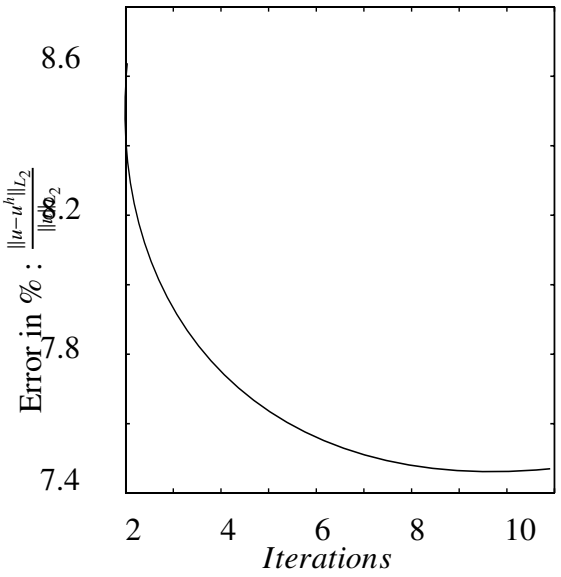

(c)

Figure 21: (a) Mesh before *r*-adaption (b) Mesh after *r*-adaption (c) Error norm variation with iterations

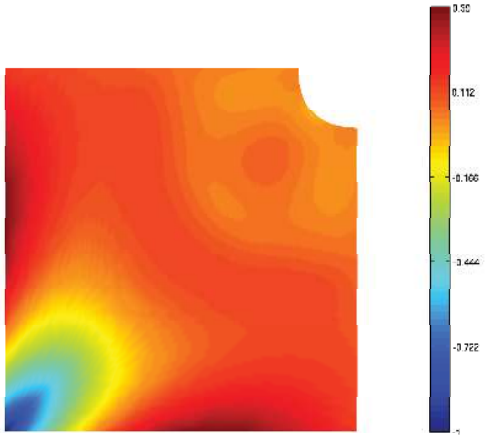

(a)

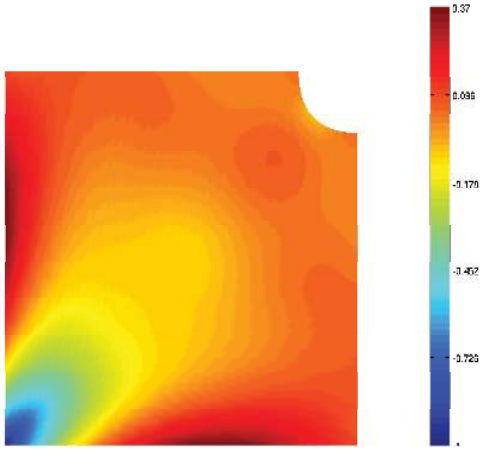

(b)

Figure 22: (a) Error plot before $r-$ adaption (b) Error plot after $r-$ adaption

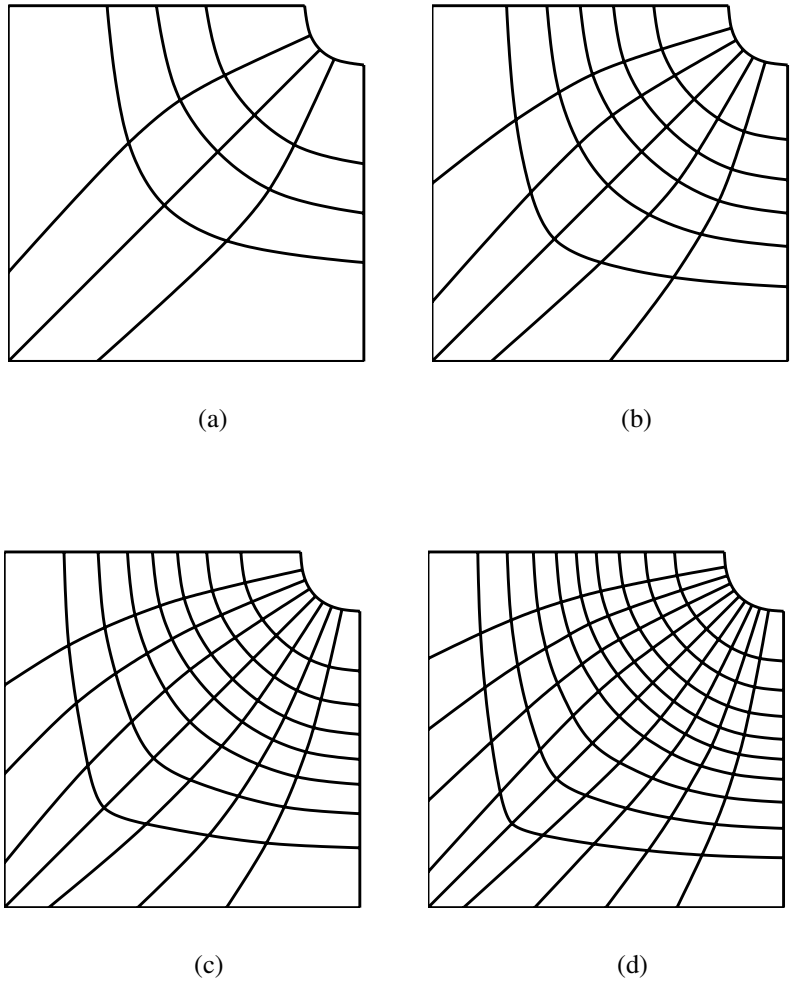

Figure 23: $h-$ adaptive refinement meshes

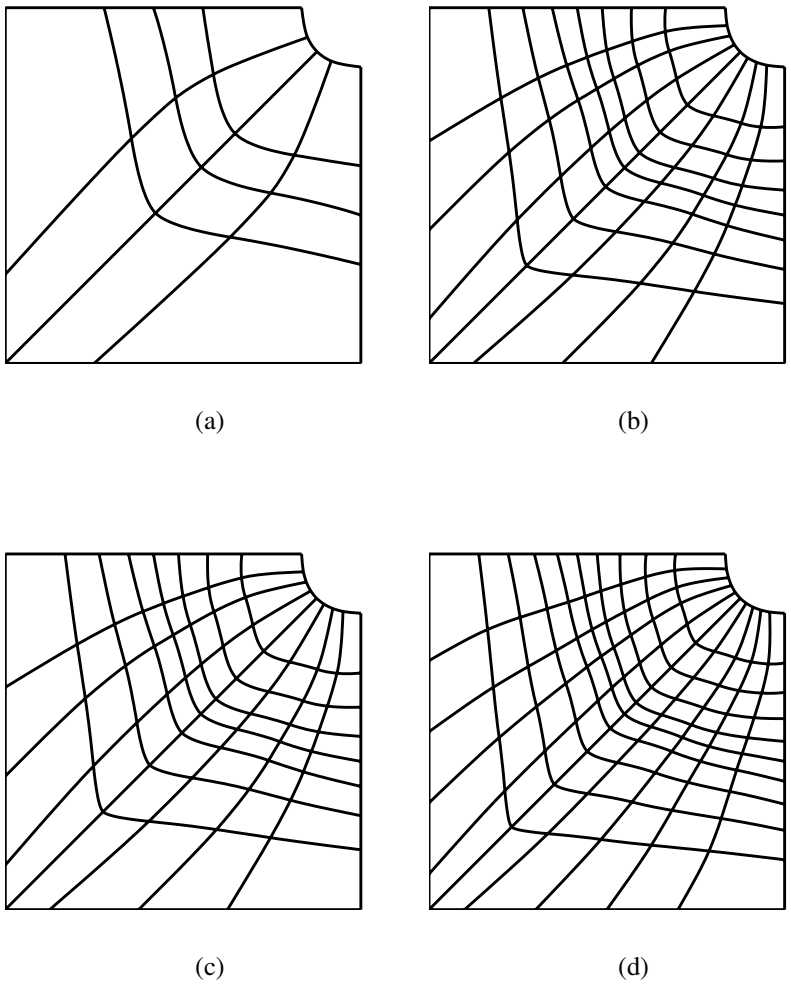

Figure 24: Combined *r*-*h* adaptive refinement meshes

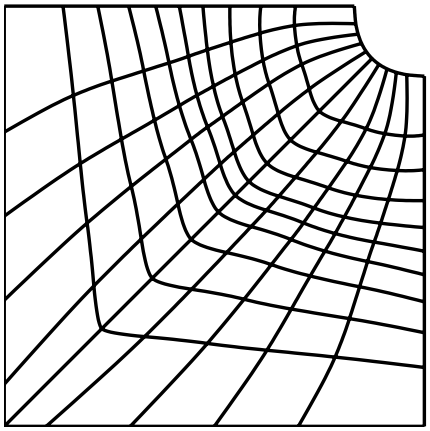

(a)

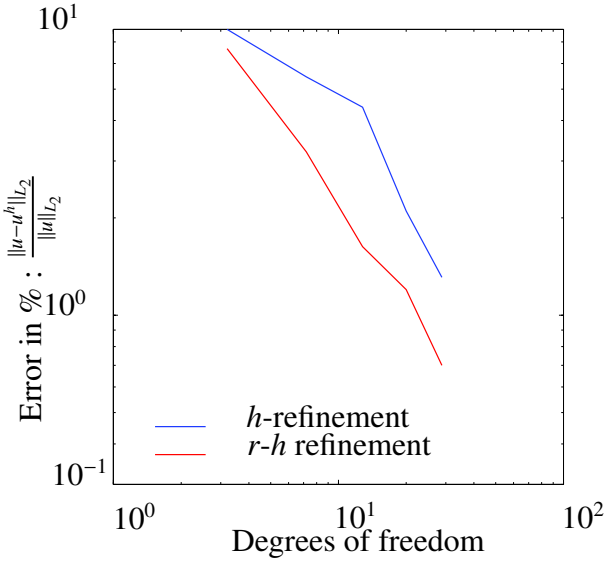

(b)

Figure 25: (a) Final mesh obtained from combined *rh* adaptive refinement meshes (b) Comparison of convergence in error norm between *h* and *r*-*h* refinements

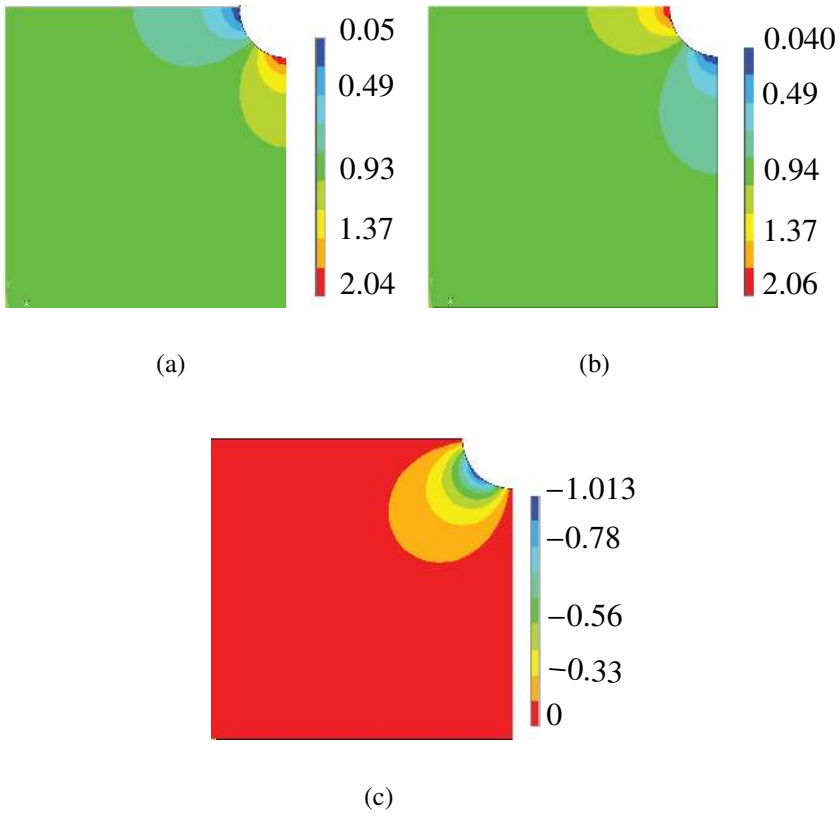

Figure 26: Plate with a hole example (a) Distribution of stress σ_{xx} (b) Distribution of stress σ_{yy} (c) Distribution of stress σ_{xy} obtained from the final adapted mesh